AN ABSTRACT OF THE THESIS OF

Brent M. Goehring for the degree of Master of Science in Geology presented on
June 6, 2006.
Title: ^{10}Be Exposure Ages of Erratic Boulders in Southern Norway and
Implications for the History of the Fennoscandian Ice Sheet.

Abstract approved:

<div style="text-align:center">

_____

Edward J. Brook

</div>

This thesis focuses on the application of the cosmogenic nuclide

Beryllium-10 (^{10}Be) in an effort to better constrain the thickness history of the

Fennoscandian Ice Sheet (FIS) at the Last Glacial Maximum (LGM) and into the

Holocene, as well as begin to answer the long-standing question regarding the age

and interpretation of periglacial weathering features in southern Norway. ^{10}Be

exposure ages of glacially transported boulders have been measured along three

vertical transects (Skåla, Blåhø, and Elgåhogna) in southern Norway. At the LGM,

^{10}Be ages indicate that ice at Blåhø and Elgåhogna was thicker than that based on

reconstructions using blockfield-weathering limits, and better agrees with models

based on ice physics or isostatic rebound inversion. Ice surface elevation at Skåla

was likely no greater than ~1440 m at the LGM, agreeing well with the mapped

trimline in that region, as well as high resolution models for Nordfjord. At all three

sites, rapid deglaciation begins at approximately 12 ^{10}Be ka, and deglaciation is

complete by approximately 9 ^{10}Be ka.

A progressive and large divergence between boulder and bedrock exposure ages is observed at the easternmost site (Elgåhogna), indicating that the bedrock has experienced minimal erosion under cold-based ice. Therefore, blockfields are not young features (< ~10 kyr), but rather have survived beneath regions of cold-based ice, possibly through multiple glacial-interglacial cycles.

^{10}Be Exposure Ages of Erratic Boulders in Southern Norway and Implications for the History of the Fennoscandian Ice Sheet

by
Brent M. Goehring

A THESIS

submitted to

Oregon State University

in partial fulfillment of
the requirements for the
degree of

Master of Science

Presented June 6, 2006
Commencement June 2007

Master of Science thesis of <u>Brent M. Goehring</u> presented on <u>June 6, 2006</u>.

APPROVED:

_____

Major Professor, representing Geology

_____

Chair of the Department of Geosciences

_____

Dean of the Graduate School

I understand that my thesis will become part of the permanent collection of Oregon State University libraries. My signature below authorizes release of my thesis to any reader upon request.

_____

Brent M. Goehring, Author

CONTRIBUTION OF AUTHORS

There are three coauthors on the manuscript presented in Chapter 1. Edward Brook provided the impetus for this project by building on previous work of his. He provided guidance with manuscript organization and completed the bulk of editing for the manuscript. Henriette Linge provided some of the data used in the interpretations of our new results. Henriette also assisted in the field and provided assistance with field logistics. Grant Raisbeck operates the Tandetron Facility at Gif-sur-Yvette and measured all of the $^{10}Be/^{9}Be$ ratios presented in this work, he also provided guidance in the final preparation of samples and confirmed that the OSU acid chemistry lab is indeed capable of producing low boron samples.

TABLE OF CONTENTS

TABLE OF CONTENTS (Continued)

LIST OF FIGURES

LIST OF TABLES

LIST OF APPENDICES

LIST OF APPENDIX FIGURES

LIST OF APPENDIX TABLES

[10]Be Exposure ages of erratic boulders in southern Norway and implications for the history of the Fennoscandian Ice Sheet

Chapter 1

Introduction

1.1 Forward

Although the margins and retreat history of the last glacial maximum (LGM) ice

sheets are fairly well constrained from field observations, the thickness and thickness

evolution of these ice sheets are not (Clark and Mix, 2002). Reconstruction of ice sheet

thickness has been limited by two problems: (1) the lack of vertical ice thickness

indicators, and (2) the lack of age control when ice thickness indicators are available.

LGM ice sheets primarily developed in regions of low topography (e.g. Laurentide, Kara-

Barents ice sheets), so there are few vertical indicators of ice sheet thickness and the

glacial deposits contain little or no information about the height of the ice in these

regions. Age control has been an issue because of the lack of radiocarbon datable

material associated with potential ice thickness indicators (glacial trimlines, moraines,

weathering zones) where they exist.

A better understanding of LGM ice sheet thickness is important for interpretation

of records of sea level change, modeling of atmospheric circulation and temperature, and

processes contributing to glacial landform development. For sea level change, the total

contribution from all LGM ice sheets is reasonably well constrained, but individual ice

sheet contributions are still tentative and largely based on isostatic rebound models (Peltier, 2004). Direct measurements of ice sheet thicknesses are required to evaluate the accuracy of these models and further constrain ice sheet contributions to sea level change. In addition to the total glacial to interglacial change in sea level, discrete meltwater events are observed in records of sea level change (Fairbanks, 1989; Bard et al., 1990; Hanebuth et al., 2000; Yokoyama et al., 2000; Clark et al., 2004). New constraints on changes of ice sheet thickness over time may be helpful for determining the source of these meltwater events and better understanding of associated climate change (Clark et al., 2004).

Better constraints on ice sheet elevation are important for climate models for the LGM. Atmospheric general circulation models (AGCMs) for the LGM require the dimensions of the major ice sheets as boundary conditions. In many models temperature near and far from ice sheets is sensitive to the presence and height of continental ice (Shinn and Barron, 1989; Ramstein and Joussaume, 1995; Felzer et al., 1996; Barron and Pollard, 2002; Pollard and Barron, 2003), while circulation and precipitation patterns are more sensitive to the areal extent of ice sheets (Manabe and Broccoli, 1985; Ramstein and Joussaume, 1995; Kageyama et al., 1999).

Finally, there are persistent questions about the formation of glacial and periglacial landscapes and their survival during glacial periods. For many areas thought to be covered by ice during the LGM there are long standing debates over the distribution and age of landforms that appear to have survived multiple glacial cycles (e.g. Kleman and Borgstrom, 1990; Kleman, 1994). A better understanding of ice sheet thickness,

which partially controls ice sheet basal temperature and therefore erosive power, will lead to a better understanding of the distribution and age of glacial and periglacial landscapes in regions thought to be covered by LGM ice sheets.

Southern Norway is an excellent area to begin to address the above questions. The region has experienced multiple glaciations during the late Cenozoic, beginning ca. 1.1 Ma (Sejrup et al., 2000). Alpine and fjord landscapes dominate the western areas near the coastline, while the central and eastern portions of southern Norway are characterized by groups of isolated peaks. The high topography of southern Norway makes it an ideal location to track the thickness of the Fennoscandian Ice Sheet (FIS). In addition to the ideal topography, accessible bedrock surfaces and glacially transported boulders make it ideal for the application of surface exposure dating.

This thesis reports ^{10}Be exposure ages of glacially transported boulders from three regions in southern Norway. Samples were taken from boulders resting on bedrock, till, and in situ fractured bedrock material. The primary goal of the study was to reconstruct the thickness of the FIS since the LGM. The results also have implications for the erosional history of the surface underlying the sampled boulders.

1.2 Summary of Chapters

Chapter 2 contains a study applying surface exposure dating to glacially transported boulders to reconstruct the thickness history of the FIS, as well as answer persistent questions regarding the age of periglacial features in southern Norway. Chapter 2 is formatted for submission to Quaternary Science Reviews. Four appendices are

included in this thesis as supplementary data. Appendix A contains a photograph and

short description of each boulder sampled. Appendix B contains tables of additional data

collected during processing and measurement of samples. Appendix C contains a

modified version of the ^{10}Be extraction procedure used here, originally developed by

Licciardi (2000). It has been updated to reflect current lab facilities at OSU, and describes

refinements of several procedures. Finally, Appendix D contains MATLAB scripts that

were used to calculate exposure ages for samples in this study. The scripts are free to be

used by anyone; however, resulting exposure ages should be checked by hand before

reporting to ensure correct execution of the scripts.

Chapter 2

[10]BE EXPOSURE AGES OF ERRATIC BOULDERS IN SOUTHERN NORWAY AND IMPLICATIONS FOR THE HISTORY OF THE FENNOSCANDIAN ICE SHEET

Brent M. Goehring [a], Edward J. Brook [a], Henriette Linge [b], and Grant Raisbeck [c]

[a] Department of Geosciences, Oregon State University, 104 Wilkinson Hall, Corvallis, Oregon 97331, USA
[b] Bjerknes Centre for Climate Research, Allégaten 55, N-5007 Bergen, Norway
[c] Centre de Spectrométrie Nucléaire et de Spectrométrie de Masse, CNRS, Bâtiment 108, F-91405 Orsay, France

2.1 Abstract

The margins of the Fennoscandian Ice Sheet (FIS) during the Last Glacial Maximum and later are fairly well constrained; however, the thickness of the FIS and its temporal evolution are poorly known. Here we present [10]Be exposure ages of glacially transported boulders along three vertical transects in southern Norway. Ice surface elevation during the LGM at our westernmost site, Skåla, was likely at approximately 1440 m, coinciding with a mapped trimline. At our central site, Blåhø, ice surface elevation at ~25 ka was at approximately the summit elevation of 1620 m. Elgåhogna, our easternmost site, likely had thick ice covering its summit during the LGM, as our data indicate that LGM ice at this location was above the summit elevation of 1460 m. A period of rapid deglaciation began at all of our sites at approximately 12 ka and the ice sheet surface was below our lowest sample by approximately 9 ka.

Our data, when combined with previous bedrock and blockfield (highly weathered bedrock on summits) exposure ages, resolves a long-standing debate over the age and geomorphic interpretation of blockfields and weathering zones in southern Norway. Frozen-bed, low-erosive ice clearly covered the summit blockfields at Blåhø, and especially at Elgåhogna, where we find a large and progressive divergence between boulder and bedrock exposure ages with elevation. Our data lead to the conclusion that the lower limit of blockfields in some areas should be interpreted as a subglacial thermal boundary, rather than the upper limit of the LGM FIS, and that blockfields have survived multiple glacial cycles. We also compare our deglaciation record with several recent time dependent ice sheet and flowline models and find that during deglaciation, models

generally match our exposure ages reasonably well, but model ice sheet height for the LGM in the time dependent models is greater than our data indicate. Ice sheet reconstructions for the LGM only, on the other hand, generally better predict LGM ice sheet elevations.

2.2 Introduction

Although the margins and retreat history of the last glacial maximum (LGM) ice sheets are fairly well constrained from field observations, the thickness and thickness evolution of these ice sheets is not (Clark and Mix, 2002). Reconstruction of ice sheet thickness has been limited by two problems: (1) the lack of vertical ice thickness indicators, and (2) the lack of age control when ice thickness indicators are available. LGM ice sheets primarily developed in regions of low topography (e.g. Laurentide, Kara-Barents ice sheets), so there are few vertical indicators of ice sheet thickness and the glacial deposits contain little or no information about the height of the ice in these regions. Age control has been an issue because of the lack of radiocarbon datable material associated with potential ice thickness indicators (glacial trimlines, moraines, weathering zones) where they exist.

A better understanding of LGM ice sheet thickness is important for interpretation of records of sea level change, modeling of atmospheric circulation and temperature, and processes contributing to glacial landform development. For sea level change, the total contribution from all LGM ice sheets is reasonably well constrained, but individual ice sheet contributions are still tentative and largely based on isostatic rebound models

(Peltier, 2004). Direct measurements of ice sheet thicknesses are required to evaluate the accuracy of these models and further constrain ice sheet contributions to sea level change. In addition to the total glacial to interglacial change in sea level, discrete meltwater events are observed in records of sea level change (Bard et al., 1990; Hanebuth et al., 2000; Clark et al., 2004). New constraints on changes of ice sheet thickness over time may be helpful for determining the source of these meltwater events and better understanding of associated climate change (Clark et al., 2004).

Better constraints on ice sheet elevation are important for climate models for the LGM. Atmospheric general circulation models (AGCMs) of the LGM require the dimensions of the major ice sheets as boundary conditions. In many models temperature near and far from ice sheets is sensitive to the presence and height of continental ice (Shinn and Barron, 1989; Ramstein and Joussaume, 1995; Felzer et al., 1996; Barron and Pollard, 2002; Pollard and Barron, 2003), while circulation and precipitation patterns are more sensitive to the areal extent of ice sheets (Manabe and Broccoli, 1985; Ramstein and Joussaume, 1995; Kageyama et al., 1999).

Finally, there are persistent questions about the formation of glacial and periglacial landscapes and their survival during glacial periods. For many areas thought to be covered by ice during the LGM there are long standing debates over the distribution and age of landforms that appear to have survived multiple glacial cycles (i.e. Kleman and Borgstrom, 1990; Kleman, 1994). A better understanding of ice sheet thickness, which partially controls ice sheet basal temperature and therefore erosive power, will lead

to a better understanding of the distribution and age of glacial and periglacial landscapes in regions thought to be covered by LGM ice sheets.

Southern Norway is an excellent area to begin to address the above questions. The region has experienced multiple glaciations during the late Cenozoic, beginning ca. 1.1 Ma (Sejrup et al., 2000). Alpine and fjord landscapes dominate the western areas near the coastline, while the central and eastern portions of southern Norway are characterized by groups of isolated peaks. The high topography of southern Norway makes it an ideal location to track the thickness of the Fennoscandian Ice Sheet (FIS). In addition to the ideal topography, accessible bedrock surfaces and glacially transported boulders make it ideal for the application of surface exposure dating.

This study reports ^{10}Be exposure ages of glacially transported boulders from three regions in southern Norway. Samples were taken from boulders resting on bedrock, till, and in situ fractured bedrock material. The primary goal of the study was to reconstruct the thickness of the FIS since the LGM. The results also have implications for the erosional history of the surface underlying the sampled boulders.

2.3 Previous Work

2.3.1 Blockfields, Weathering Zones, and FIS Geometry

Blockfields, also known as felsenmeer, are a chaotic assemblage of fractured bedrock found on the summits and high plateaus of mountains in mid- and high-latitude regions (Fairbridge, 1968). The appearance of a blockfield can best be described as a sea of jagged boulders and rock fragments. Blockfield formation possibly occurs via frost

shattering of massive well-jointed bedrock. Nesje et al. (1987) mapped the geographical and vertical distribution of blockfields in southern Norway. They found the largest blockfield concentration near the Jotunheimen Mountains (Figure 2.1), and extensive blockfields were also found in the Nordfjord-Møre region of southwestern Norway. Blockfields are also found in the Dovre and Rondane Mountains in south-central Norway, as well as around Lake Femunden near the Norway-Sweden border.

The age of blockfields on the summits of many Norwegian peaks has been debated for decades (Dahl, 1966a, 1966b; Nesje et al., 1987; Nesje et al., 1988; Nesje et al., 1994; Rea et al., 1996). Dahl (1966a; 1966b) argued for blockfield formation after the disappearance of the FIS at the end of the last ice age. Nesje et al. (1987, 1988) and Nesje and Dahl (1990) argued that blockfields pre-date the LGM and that their lower limit can be used as an ice thickness indicator. Using this argument, Nesje et al. (1988) reconstructed a thin LGM FIS that reached its maximum thickness near the current drainage divide along the Jotunheimen Mountains, and thinned significantly to the east. In support of this position, McCarroll and Nesje (1993) and Nesje et al. (1994) used a micro-roughness meter to map vertical weathering zones. They found that surfaces above the blockfield boundary were considerably rougher than surfaces below, suggesting longer exposure to weathering, supporting the argument that the blockfield boundary represents the LGM ice sheet limit.
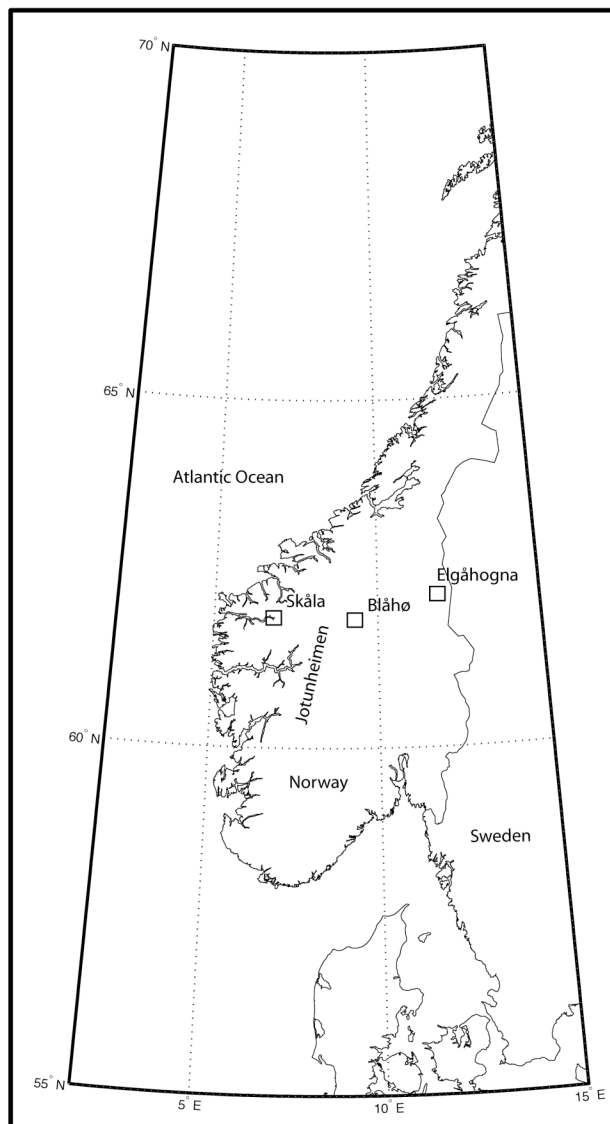
Figure 2.1. Map of southern and central Norway showing areas in this study. Sample locations for each study area shown in Figure 2.3.

In contrast, reconstructions based on a variety of ice sheet models suggest that ice at the LGM covered most, if not all of the summits in southern Norway (Follestad, 1990).

Models of the FIS constructed via inversion of crustal isostatic rebound patterns and sea level (Peltier, 1994; Peltier, 2004), 3-D thermo-mechanical ice sheet models (Näslund et al., 2003; Siegert and Dowdeswell, 2004), ice sheet surfaces based on the distribution of glacial geologic evidence (Boulton et al., 1985), and the CLIMAP maximum model of Hughes (1981) support a thick LGM FIS. Such models can account for the distribution of blockfields through survival beneath cold-based, low-erosive ice or formation after the retreat of the LGM FIS.

Our study areas (Figure 2.1) are ideally situated to test the various reconstructions of the FIS. Figure 2.2 shows ice sheet profiles along 62°N for the LGM based on the thin ice sheet reconstruction of Nesje and coworkers, as well as multiple thicker ice sheet models discussed above. At our three field sites, the reconstruction of Nesje and coworkers predicts LGM ice elevations below the summits, while most of the ice sheet models predict ice elevations above the summits of Blåhø and Elgåhogna. Only one model, ICE-4G (Peltier, 1994), predicts ice elevations higher than all summits in our study.
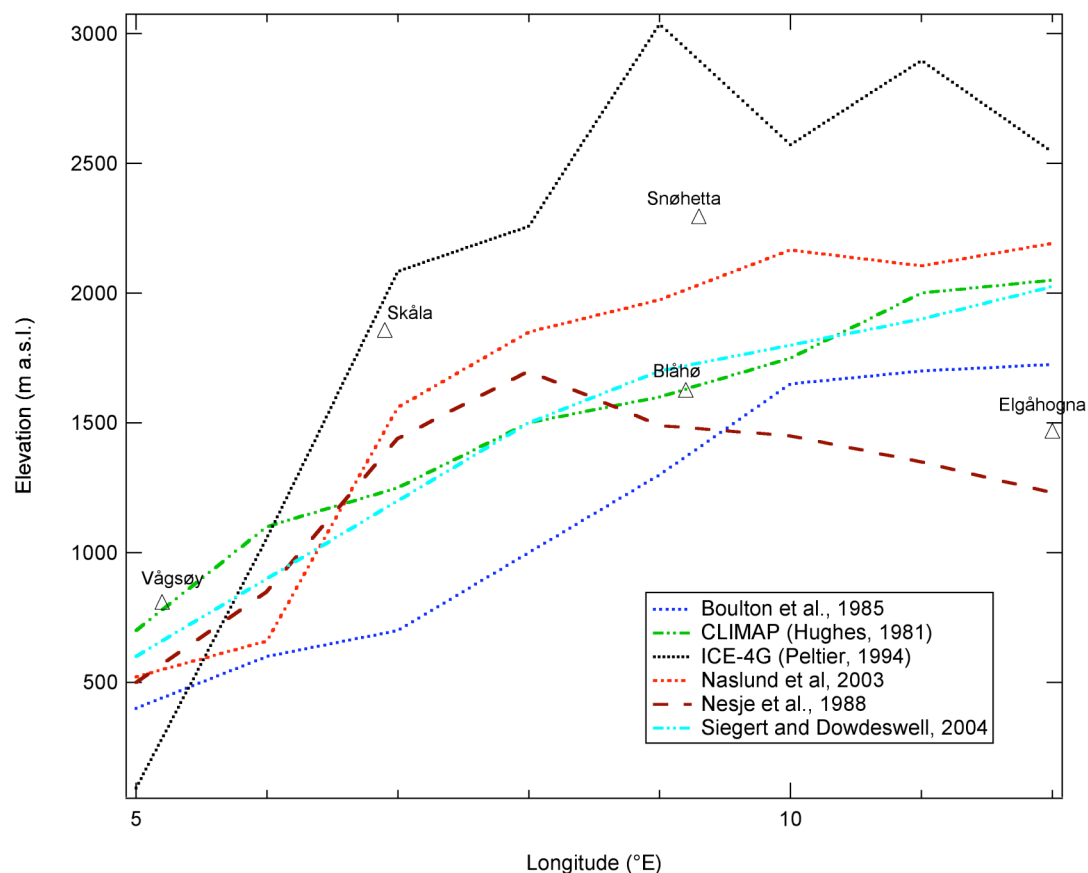
Figure 2.2. Profiles of LGM FIS elevation reconstructions along 62°N for 21 ka. Elevations at each location are either extracted from the nearest grid cell in model output, or are taken from contour maps of the reconstructed ice surface. Note the nearly 1500 m difference in ice sheet elevation predicted by Nesje et al., 1988 and ICE-4G models at Blåhø and Elgåhogna; others sites and models also have large differences.

2.3.2 Bedrock Exposure Ages

Brook et al. (1996, in prep) and Linge et al. (2006) reported exposure ages for bedrock and blockfield surfaces at Skåla, Blåhø, and Elgåhogna. At all three sites, bedrock exposure ages generally increase with elevation up to either the summit or blockfield boundary. In some cases summit exposure ages are younger than surfaces from just below the summit. Results within blockfields show more scatter, including very

young and in some cases very old, exposure ages, however most ages within the

blockfield predate the LGM. These bedrock and blockfield exposure ages allow for either

protrusion of blockfield-mantled summits through the ice sheet as nunataks or complete

cover by cold-based ice that either did not erode or did not sufficiently erode blockfield

surfaces to reset the "cosmogenic clock". Because bedrock ages do not provide

conclusive results, we use the alternate approach of dating boulders here, and compare

bedrock and boulder exposure ages to learn about the ice sheet and geomorphic history of

southern Norway.

2.4 Methods

2.4.1 Sampling Strategy

Exposure ages using cosmogenic nuclides offer a way to determine the thickness

of ice sheets by dating glaciated surfaces, boulders, or other deposits that have been

modified or transported by a former ice sheet. Several studies have attempted to

determine LGM ice sheet thickness for the FIS, British Isles Ice Sheet, Laurentide Ice

Sheet, and West Antarctic Ice Sheet by dating glacially modified bedrock (Brook et al.,

1996; Stone et al., 1998; Marquette et al., 2004; Linge et al., 2006) and boulders (Ackert

et al., 1999; Stone et al., 2003; Briner et al., 2006). A number of studies suggest that

using bedrock surfaces in this way is problematic because they can retain a record of

"previous exposure" (Briner and Swanson, 1998; Steig et al., 1998; Bierman et al., 1999;

Colgan et al., 2002; Fabel et al., 2002; Stroeven et al., 2002; Briner et al., 2006; Linge et

al., 2006). The probable explanation for these results is that glacial erosion was insufficient to reset the "cosmogenic clock" and a record of previous exposure remained.

Although the prior exposure problem can also arise when using glacially transported boulders, it seems much more acute when using bedrock. Studies using glacially transported boulders produce more consistent ages, and only occasional "outliers" are encountered (e.g. Gosse et al., 1995a, 1995b; Briner et al., 2006). Briner (2003) provided a clear demonstration of the bedrock exposure age problem by showing that ages of boulders and underlying bedrock can differ significantly. Similar results for our eastern site are presented below. Their data set of exposure ages of glacially transported boulders supports the use of boulders over bedrock to constrain the thickness of former ice sheets, especially in regions where erosion may not have been sufficient to reset the cosmogenic clock.

In this study, glacially transported boulders were sampled along vertical transects at several sites in southern Norway. The logic behind the sampling is that the elevation of boulder deposition records paleo-ice thickness. Exposure ages for a boulder then provides the age of deglaciation of the site. Three peaks (Skåla, Blåhø, and Elgåhogna) from the western, central, and eastern regions of southern Norway (Figure 2.1) were chosen because of the presence of boulders, the greatest amount of relief above the surrounding topography, and availability of bedrock and blockfield exposure ages from previous studies.

2.4.2 Field Areas

Skåla

Skåla (61.8°N, 6.9°E; 1848 m a.s.l.) is located in the western region of southern Norway near Loen in inner Nordfjord (Figures 2.1, 2.3). This site provides an excellent opportunity to track the thickness of the FIS since the LGM as Skåla has the largest vertical relief of any peak in Norway. The summit is mantled by a blockfield, extending down to approximately 1560 m. Further down slope at approximately 1440 m a lower trimline can be identified by a change in rock color and a discontinuous line of boulders (McCarroll and Nesje, 1993; Brook et al., 1996). At approximately 1100 m, a Younger Dryas (YD) lateral moraine forms a clear ridge (Nesje and Dahl, 1992). The bedrock at Skåla is ca. 1031 Ma quartz monzonite and augen gneiss, typical of the bedrock in the greater Nordfjord region (Sigmond et al., 1984).

A total of twelve boulders were sampled along a vertical transect on Skåla over an elevation range from 760 to 1384 m (Figure 2.3a). Duplicate samples were collected at 1384 m, 1244 m, 1220 m, and 1028 m. Boulder lithology was consistently augen gneiss. Unfortunately, no appropriate boulders could be located above 1384 m. Boulder size ranged from less than 1 m^3 up to ~ 15 m^3. Some larger boulders were also sampled at lower elevations beneath the steep northern slope; however, these appear to be the result of rock fall, as their exposure ages appear to be too young for glacial deposition.
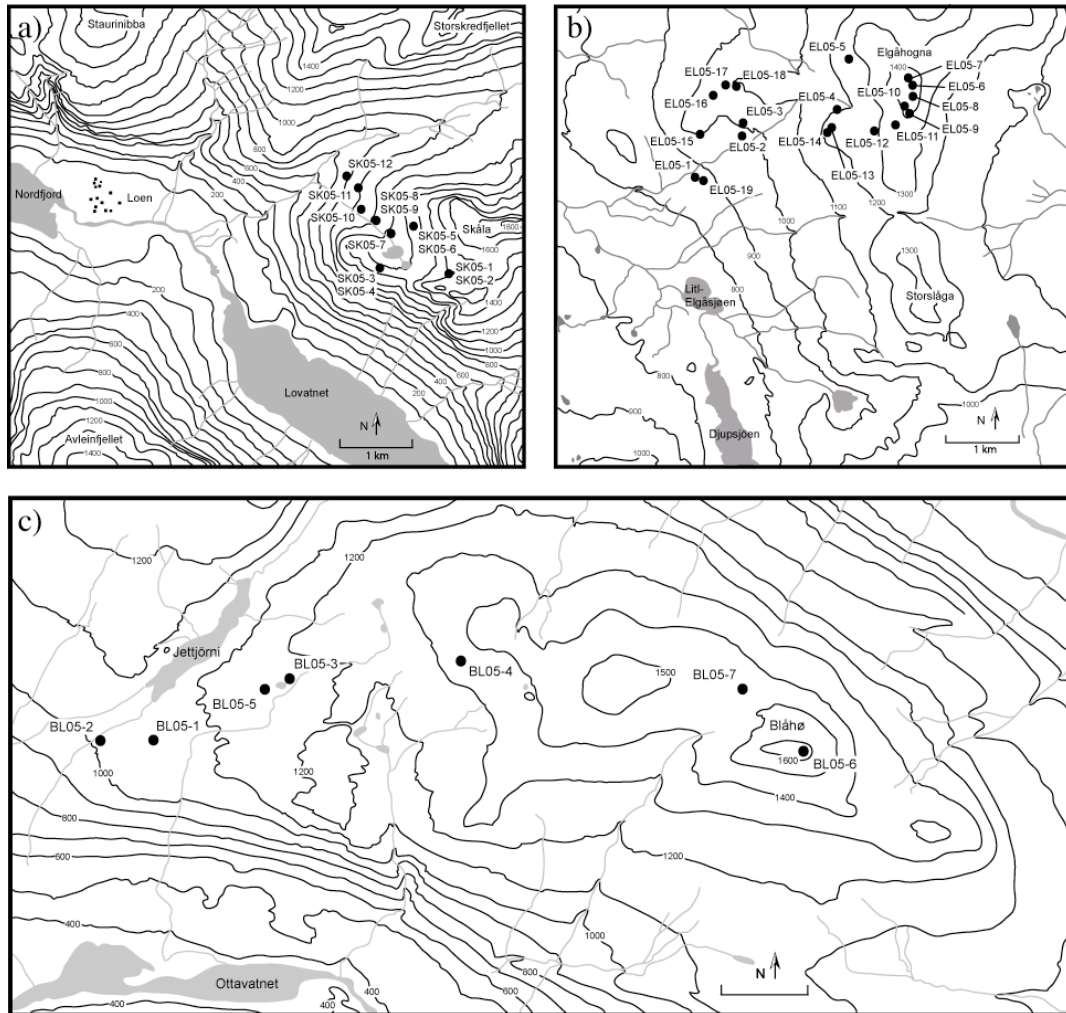
Figure 2.3. Sample location maps for each area in this study (see Figure 2.1), modified from 1:50000 topographic maps. a) Skåla, b) Elgåhogna, c) Blåhø. Contour interval is 100 m.

Blåhø

Blåhø is located in central southern Norway (61.8°N, 9.2°E; 1617 m a.s.l.) north of Ottavatnet (Figures 2.1, 2.3). The Blåhø summit is near the intersection of two major valleys that previously served as major drainages as the FIS retreated. The lower slopes of Blåhø are characterized by exposed bedrock surfaces displaying glacial striations and

chatter marks that indicate the presence of sliding ice. Above approximately 1450 m the surface is mantled by a blockfield, and between 1200 and 1450 m a thin till sheet covers the surface, with outcropping areas of bedrock. Two bedrock lithologies are present at Blåhø, meta-conglomerate at higher elevations and meta-sandstone on the lower slopes (Sigmond et al., 1984).

Seven glacially transported boulders were sampled for [10]Be analysis (Figure 2.3c). Sample elevations range from 1086 m to 1617 m. The three lowest samples rest on striated bedrock, three intermediate elevation samples are taken from boulders resting on bedrock and till, and one sample was collected from the blockfield. The sample collected from the blockfield was distinguished from the underlying blockfield material by its rounded morphology and erratic lithology. Five of the samples are meta-sandstone, and the remaining two are quartz pegmatites that are clearly not locally derived.

Elgåhogna

Elgåhogna (62.1°N, 12.0 °E; 1460 m a.s.l.) is located in southeastern Norway just east of the lake Femunden (662 m a.s.l; Figure 2.1). The region around Elgåhogna has extensive till cover likely deposited during the LGM. The summit of Elgåhogna is quite broad and is mantled by blockfield material above approximately 1200 m. Bedrock in the region is dominantly pink and gray arkosic sandstone that has nearly reached quartzite grade. Rare pockets of foliated granites and feldspathic conglomerates also occur.

Eighteen boulders were sampled for [10]Be exposure ages at Elgåhogna between elevations of 880 and 1460 m (Figure 2.3b). The slopes of Elgåhogna are littered with boulders of varying sizes. All boulders sampled at this location were greater than 1 m^3

and many were clearly erratics based on lithology. Sixteen were pink and gray quartzites, while two were quartz-poor feldspathic conglomerates. Sampled boulders rest on bedrock, blockfield material, or till.

2.4.3 Sampling Methods

We sampled boulders interpreted to be glacially transported for ^{10}Be exposure age chronology (Figure 2.4). Determination of transport by glaciers was made based on boulder morphology, lithology, and geomorphology of the surrounding topography. Boulders resting on glacially striated or polished bedrock were sampled in preference to boulders resting on unconsolidated material. Rounded boulders and/or boulders with glacial tool marks were sampled in preference to boulders not displaying these characteristics, and preference was given to erratic boulders with lithology unlike the surrounding bedrock. Boulders greater than ~1m^3 were sampled where possible, minimizing the likelihood of post-depositional movement; only one sample (BL05-6) did not meet the size criterion.

Boulders were sampled with hammer and chisel. Rock chips were taken from the top of each boulder, preferably from horizontal or shallowly dipping surfaces, minimizing slope effects. Boulder substratum was noted (bedrock, sediments, or blockfield). At each sampling location, the latitude and longitude were recorded using handheld GPS units and elevation obtained using barometric altimeters (± 5m) calibrated daily to local benchmarks; elevations were subsequently checked using topographic

maps. Topographic shielding was measured using compass and inclinometer at 10°

intervals of azimuth.
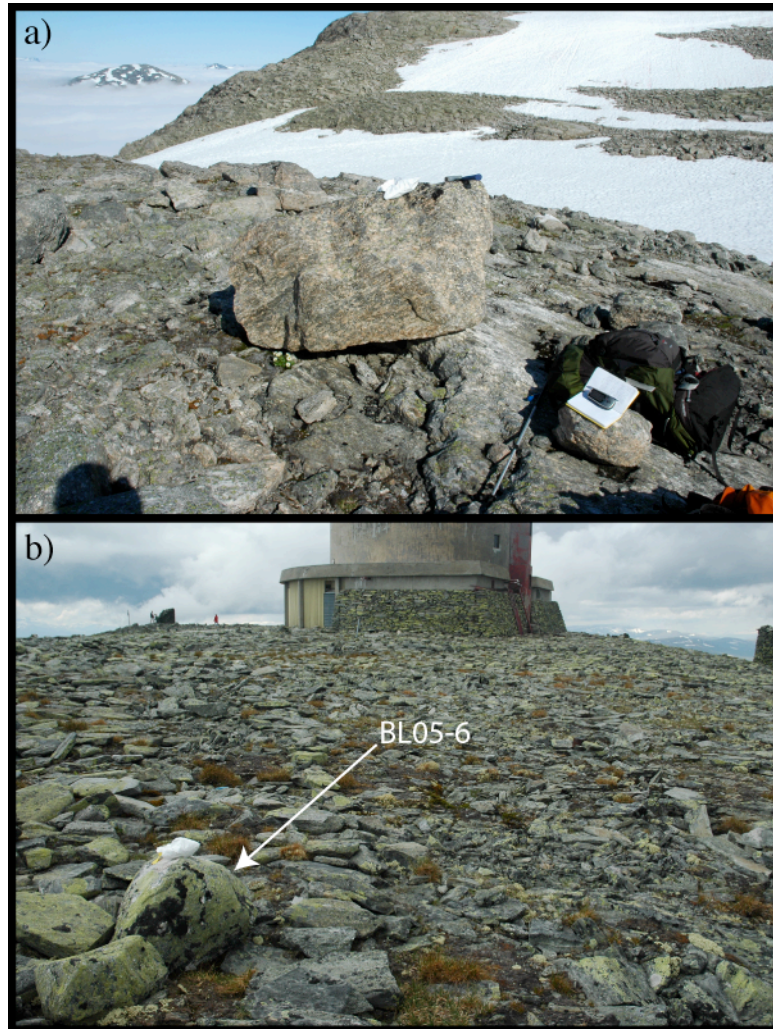
Figure 2.4. a) Typical boulder at Skåla, sample SK05-1. Boulder SK05-1 lithology is quartz-feldspar augen gneiss and rests on bedrock in a late-glacial cirque. b) Summit blockfield at Blåhø with sample BL05-6 shown (see arrow). BL05-6 is quartz pegmatite and is also the smallest boulder sampled in this study.

2.4.4 Analytical Methods

Samples were prepared at Oregon State University following methods of Licciardi (2000), slightly modified by Goehring (2006) and described in Appendix C. Samples were crushed using a large Braun Chipmunk jaw crusher and subsequently pulverized using a variable width Bico disk mill. The 250-710 μm fractions were isolated using standard testing sieves. A powerful hand magnet was used to remove highly magnetic minerals and samples were further purified using a Frantz Isodynamic Mineral Separator to remove weakly magnetic minerals. After the majority of magnetic minerals were removed, the sample was repeatedly leached (>3 times) for 24 hrs per leach in 1% hydrofluoric (HF)/1% nitric acid (HNO_3) in a warm (~60°C) ultrasonic bath to dissolve all non-quartz minerals as well as remove meteoric ^{10}Be from the quartz surface. Between each leaching the samples were rinsed three times with ultrapure water, and new acid solution was added to the leaching bottles. When samples appeared visually pure, quartz purity was checked further via measurements of Al, K, Na, Fe, Ti, Ca, Mg by inductively coupled plasma-optical emission spectroscopy (ICP-OES). Samples were accepted for further processing when all measured cation concentrations were below 500 ppm. Samples with any cation concentrations greater than 500 ppm were leached for an additional 24-48 hrs.

Once sufficient purity was obtained, ~10 to 50 g of sample was added to a Teflon jar and ~250 μg Be carrier was added to each sample (most samples were > 20 g; only two were < 10 g due to low quartz content of the starting material). Samples were then dissolved in concentrated HF. The HF was evaporated and successive perchloric ($HClO_4$)

and hydrochloric acid (HCl) evaporations were completed to drive off fluorides and convert the sample to chloride form. Beryllium was extracted from each sample via anion and cation exchange. Following cation exchange, the sample was brought up to ~pH 5 to remove any Ti remaining in the sample by precipitating as titanium hydroxide. After centrifugation and removal of any Ti precipitate if present, ammonium hydroxide (NH_4OH) was added until the sample reached ~pH 8 and beryllium hydroxide ($Be(OH)_2$) precipitated. The precipitate was rinsed three times in ultrapure pH 8 water to remove boron. Samples were then redissolved in 10% HNO_3, transferred to nitric acid cleaned quartz crucibles, and evaporated. $Be(NO_3)_2$ was then converted to beryllium oxide (BeO) by heating covered quartz crucibles in a rapid mineralizer (LHG Schnellverascher) set at 999°C for one hour.

$^{10}Be/^9Be$ ratios were measured by accelerator mass spectrometry (AMS) at the IN2P3 Tandem Accelerator Facility at Gif-sur Yvette, France (Raisbeck et al., 1994) relative to the NIST standard (SRM 4325) with a certified $^{10}Be/^9Be$ ratio of 26.8 ± 1.4 x 10^{-12}. Uncertainties (1σ) in ^{10}Be concentration were calculated based on counting statistics combined in quadrature with a 5% long-term machine uncertainty. Blank corrections were made by reducing the number of ^{10}Be atoms in each sample by the error weighted mean of seven full procedural blanks (5.45 ± 0.35 x 10^4 ^{10}Be atoms) and blank uncertainty was incorporated into the final sample concentration.

Corrections for sample thickness were made assuming an exponential decrease in production rate with depth and a 155 g cm^{-2} attenuation length (Brown et al., 1992). Corrections for topographic shielding were made following the methods described in

Dunne et al. (1999). Total production rate corrections for topographic shielding and sample thickness were never greater than 5%, less than the total analytical uncertainties.

^{10}Be exposure ages were calculated using a production rate of 5.1 atoms g^{-1} yr^{-1} for sea level (1013.25 hPa), high latitude (>60°) samples. Production rates for neutrons and muons were scaled independently assuming that at sea level 97.8% of production is due to neutrons and 2.2% due to muons (Stone, 2000). Sample elevation was converted to atmospheric pressure using the equation for the standard atmosphere given in Stone (2000). Production due to neutrons was then scaled for geomagnetic latitude and elevation above modern sea level using the polynomials given by Lal (1991) and adjusted for atmospheric air pressure by Stone (2000). Production by muons was scaled for altitude and latitude using the exponential equation and latitude coefficients presented in Nishiizumi et al. (1989) assuming a 242 g cm^{-2} atmospheric attenuation factor. All samples in this study come from geomagnetic latitudes >60° N for at least the last 20 kyr, thus no corrections for geomagnetic shielding were necessary (Pigati and Lifton, 2004). Finally, production rates were reduced by 14% to account for the measured difference (Middleton et al., 1993) between the ^{10}Be/^{9}Be ratio for the NIST standard used at Gif-sur Yvette and the ICN standard used to determine the ^{10}Be production rate of Lal (1991) and Stone (2000). Reported uncertainty in exposure age includes analytical uncertainty only.

2.4.5 Correction for isostatic depression/rebound

A unique aspect of working in regions formerly covered by a large ice sheet is the influence of isostatic depression and the associated uplift following ice sheet removal on

[10]Be production rate. Generally, exposure ages from these regions have not been corrected for the time-dependent production rates due to changes in atmospheric depth, with exceptions in recent studies along the southern margin of the FIS (Rinterknecht et al., 2004; Rinterknecht et al., 2006) and in the Labrador sector of the Laurentide ice sheet (Carlson et al., in prep).

We use the crustal change model of Påsse (1997), presented in Morén and Påsse (2001), to model the elevation and [10]Be production rate history of our sites for the past 60 kyr. Production rates at each time step are calculated from the resulting elevation predicted by the crustal change model and are adjusted for topography, sample thickness, and ICN/NIST differences. The resulting production rate history for each sample location is then used to predict [10]Be concentration and determine age by varying exposure age until the modeled concentration matched the measured concentration. The magnitude of correction for individual samples varies depending on the sample location, elevation, and measured concentration. Corrections are as little as 2% for a young low elevation sample from Skåla, and as great as 20-23% for 18-20 ka samples from Blåhø and Elgåhogna. Uplift curves are based on Weichselian ice extent (Mangerud, 1991) and eustatic sea level (Shackleton, 1987; Lundberg and Ford, 1994), and are uncertain beyond 10 ka. Because they are difficult to quantify we do not include these uncertainties in the exposure age uncertainties. A rough estimate is that the total isostatic depression is uncertain to ± 10%. The impact on the exposure age uncertainty depends on factors mentioned above, for the oldest samples the additional uncertainty added to the exposure age is ~ 5%. Both uncorrected and uplift/depression corrected [10]Be exposure ages are

reported in Table 2.1. Throughout the discussions below we use the corrected exposure ages. Additionally, until a firm consensus on the ^{10}Be production rate is available and geomagnetic effects are better understood, all ages should be considered ^{10}Be ages, rather than calendar ages.

2.5 Results and Discussion

2.5.1 Results

Skåla

Exposure ages for samples collected from Skåla (SK05 samples) are shown in Table 2.1 and Figure 2.5a. Duplicate samples at 1384 m have ages of 12.4±0.8 and 12.4±0.9 ka; these are the highest samples collected from Skåla. Duplicate samples from 1244 m, and slightly lower at ~1220 m, have exposure ages of 5.9±0.7 and 11.9±0.8 ka and 9.9±0.9 and 10.1±0.9 ka, respectively. One sample from 1118 m has an age of 10.7±0.9 ka. Two samples taken from 1028 m have ages of 14.4±1.0 and 9.4±0.8 ka. The three samples from elevations between 947 m and 761 m have ages of 1.4±0.4, 1.3±0.3, and 9.8±1.0 ka.

Blåhø

Exposure ages from Blåhø (BL05 samples) are shown in Table 2.1 and Figure 2.5b. The sample from the summit blockfield, at 1617 m, has an exposure age of 20.6±1.5 ka. At 1481 m, just below the blockfield boundary, an exposure age of 22.9±1.4 ka is obtained, and at 1302 m, 24.9±1.5 ka. A pair of samples from 1182m and 1176 m yielded exposure ages of 13.4±1.0 and 11.4±0.8 ka, respectively. A sample from 1142 m

has an exposure age of 9.2±2.2 ka and the lowest sample (1086 m) has an exposure age of 10.8±1.0 ka.

Elgåhogna

The eighteen exposure ages (EL05 samples) from Elgåhogna are shown in Table 2.1 and Figure 2.5c. Three samples from the summit blockfield at 1460 m have ages of 9.2±0.7, 11.5±0.8, and 13.5±1.0 ka. A sample from a bench below the summit at 1407 m has an age of 14.8±1.0 ka. One sample from 1349 m has an exposure age of 14.9±0.9 ka. Four samples between 1284 m and 1222 m have exposure ages of 13.8±0.9, 14.2±0.9, 9.1±0.6, and 11.1±0.8 ka. Samples at 1185 and 1101 m have exposure ages of 10.2±1.1 ka and 10.6±0.7 ka. Four samples from 1077m to 1009m have exposure ages of 18.9±1.1, 10.6±0.8, 13.0±1.2, and 11.2±0.7 ka. The three lowest samples, from 970m to 879 m, have exposure ages of 11.6±0.8, 10.1±0.7, and 13.6±0.9 ka.

Table 2.1. Sample information and ^{10}Be data used to calculate standard exposure ages and uplift/subsidence corrected exposure ages.
[a.] ^{10}Be concentrations have been corrected for ^{10}Be concentrations in 7 full procedural blanks with an average of 5.45 ± 0.35 x 10^4 ^{10}Be atoms.
[b.] Production rate has been scaled for neutrons and muons independently using Stone (2002) and Nishiizumi et al. (1989) respectively. Production rate shown does not include corrections for topography or sample thickness.
[c.] Corrections for shielding of cosmic rays by surrounding topography are made following Dunne et al. (1999); samples with no topographic correction have a value of 1. Corrections for sample thickness are made assuming an exponential decrease in production with depth assuming an attenuation length of 155 g cm^{-2} and sample density of 2.6 g cm^{-3}.

Table 2.1

Sample	Latitude N (DD)	Longitude E (DD)	Altitude (m a.s.l.)	Weight (g clean qtz)	[^{10}Be] Corrected [a] (10^5 atoms/ g qtz)
Skåla					
SK05-12	61.8770	6.9237	761	26.424	0.87 ± 0.09
SK05-11	61.8736	6.9252	885	26.392	0.13 ± 0.03
SK05-10	61.8701	6.9259	947	25.816	0.15 ± 0.04
SK05-8	61.8687	6.9294	1028	18.887	1.05 ± 0.09
SK05-9	61.8687	6.9294	1028	44.573	1.62 ± 0.11
SK05-7	61.8670	6.9330	1118	17.965	1.27 ± 0.11
SK05-4	61.8619	6.9357	1220	27.838	1.33 ± 0.12
SK05-3	61.8619	6.9357	1223	25.713	1.30 ± 0.11
SK05-5	61.8677	6.9389	1244	20.247	1.60 ± 0.11
SK05-6	61.8677	6.9389	1244	16.293	0.79 ± 0.09
SK05-1	61.8618	6.9500	1384	25.508	1.85 ± 0.13
SK05-2	61.8618	6.9500	1384	55.502	1.86 ± 0.11
Blåhø					
BL05-2	61.89784	9.13809	1086	30.524	1.25 ± 0.11
BL05-1	61.89590	9.14320	1142	25.034	1.14 ± 0.27
BL05-3	61.90444	9.17181	1176	30.599	1.48 ± 0.10
BL05-5	61.90289	9.16580	1182	25.015	1.74 ± 0.14
BL05-4	61.90355	9.20972	1302	30.477	3.49 ± 0.21
BL05-7	61.90295	9.25299	1481	37.529	3.77 ± 0.23
BL05-6	61.89768	9.28446	1617	25.297	3.77 ± 0.27
Elgåhogna					
EL05-19	62.1374	12.0107	879	49.129	1.33 ± 0.09
EL05-1	62.1378	12.0100	880	50.478	1.00 ± 0.07
EL05-2	62.1420	12.0182	970	51.693	1.25 ± 0.09
EL05-15	62.1426	12.0121	1009	50.395	1.23 ± 0.08
EL05-3	62.1440	12.0208	1019	13.217	1.46 ± 0.13
EL05-16	62.1476	12.0136	1038	50.587	1.19 ± 0.08
EL05-17	62.1501	12.0182	1077	50.502	2.25 ± 0.14
EL05-18	62.1491	12.0198	1101	50.504	1.28 ± 0.09
EL05-4	62.1460	12.0464	1185	7.916	1.32 ± 0.14
EL05-14	62.1434	12.0438	1222	30.252	1.49 ± 0.11
EL05-13	62.1434	12.0443	1242	49.973	1.23 ± 0.09
EL05-5	62.1519	12.0497	1278	50.976	1.99 ± 0.12
EL05-12	62.1429	12.0516	1284	49.447	1.93 ± 0.12
EL05-11	62.1436	12.0612	1349	55.191	2.20 ± 0.14
EL05-9	62.1455	12.0653	1407	30.529	2.31 ± 0.15
EL05-7	62.1494	12.0643	1460	25.053	2.18 ± 0.16
EL05-8	62.1484	12.0653	1460	51.571	1.47 ± 0.11
EL05-6	62.1489	12.0653	1461	30.834	1.86 ± 0.13

Table 2.1 cont.

Sample	Scaling Factors		Production Rate [b]	Corrections [c]		[10]Be Age	Uplift Corrected Age
	Neutrons	Muons	atoms g^{-1} yr^{-1}	Shielding	Thickness	ka	ka
Skåla							
SK05-12	2.09	1.44	10.59	0.98	0.98	9.75±0.97	10.37±1.03
SK05-11	2.32	1.52	11.74	0.99	0.97	1.32±0.30	1.35±0.31
SK05-10	2.45	1.57	12.40	0.98	0.98	1.39±0.39	1.47±0.41
SK05-8	2.62	1.63	13.25	0.98	0.98	9.44±0.80	9.93±0.84
SK05-9	2.62	1.63	13.25	0.98	0.99	14.44±1.02	16.17±1.14
SK05-7	2.82	1.69	14.26	0.99	0.96	10.73±0.93	11.39±0.99
SK05-4	3.07	1.77	15.51	0.99	0.98	10.11±0.87	10.69±0.92
SK05-3	3.08	1.77	15.56	0.99	0.98	9.85±0.86	10.40±0.91
SK05-5	3.13	1.79	15.81	0.98	0.99	11.94±0.81	12.86±0.88
SK05-6	3.13	1.79	15.81	0.98	0.99	5.90±0.65	6.08±0.67
SK05-1	3.5	1.9	17.67	0.99	0.98	12.36±0.89	13.35±0.97
SK05-2	3.5	1.9	17.67	0.99	0.98	12.42±0.75	13.43±0.82
Blåhø							
BL05-2	2.75	1.67	13.90	1	0.95	10.82±0.96	11.66±1.03
BL05-1	2.88	1.71	14.56	1	0.97	9.21±2.16	9.77±2.29
BL05-3	2.96	1.74	14.96	1	0.99	11.44±0.79	12.40±0.86
BL05-5	2.98	1.74	15.06	1	0.99	13.38±1.05	15.02±1.17
BL05-4	3.28	1.84	16.57	1	0.98	24.69±1.51	30.31±1.85
BL05-7	3.78	1.98	19.08	1	0.99	22.92±1.39	28.02±1.70
BL05-6	4.2	2.1	21.18	1	0.99	20.61±1.46	25.08±1.77
Elgåhogna							
EL05-19	2.31	1.52	11.69	1	0.96	13.57±0.92	16.04±1.08
EL05-1	2.31	1.52	11.69	1	0.97	10.08±0.68	10.95±0.74
EL05-2	2.5	1.58	12.65	1	0.98	11.55±0.80	12.91±0.89
EL05-15	2.58	1.61	13.05	1	0.96	11.24±0.74	12.46±0.82
EL05-3	2.6	1.62	13.15	1	0.98	12.97±1.16	15.00±1.34
EL05-16	2.64	1.63	13.35	1	0.96	10.63±0.75	11.62±0.82
EL05-17	2.73	1.66	13.80	1	0.99	18.88±1.14	24.71±1.49
EL05-18	2.78	1.68	14.05	1	0.98	10.64±0.74	11.61±0.81
EL05-4	2.98	1.74	15.06	1	0.98	10.24±1.09	11.09±1.18
EL05-14	3.07	1.77	15.51	1	0.99	11.11±0.78	12.21±0.86
EL05-13	3.12	1.79	15.76	1	0.99	9.02±0.63	9.61±0.67
EL05-5	3.22	1.82	16.26	1	0.99	14.16±0.85	16.82±1.01
EL05-12	3.23	1.82	16.31	1	0.98	13.83±0.86	16.24±1.01
EL05-11	3.41	1.87	17.22	1	0.98	14.94±0.92	18.10±1.12
EL05-9	3.57	1.92	18.02	1	0.99	14.83±0.99	17.89±1.19
EL05-7	3.71	1.96	18.72	1	0.99	13.47±0.99	15.57±1.14
EL05-8	3.72	1.97	18.78	1	0.97	9.24±0.72	9.87±0.77
EL05-6	3.72	1.97	18.78	1	0.99	11.46±0.80	12.67±0.89

2.5.2 Interpretation of Boulder Exposure Ages

In addition to analytical uncertainties, exposure ages of boulder surfaces are subject to geological factors such as post-depositional movement, erosion of the boulder surface, and snow cover. As discussed above, measures were taken during sampling to minimize the impact of these factors. In addition, multiple boulders from the same or similar elevation were sampled when possible. We examine our distribution of ages at each site for notable outlying points, and consider the following likely explanations for outliers (Figure 2.5).

When samples are anomalously younger than the majority of samples (e.g. SK05-6, SK05-10, SK05-11), we infer that the sampled boulder has rotated, exposing a surface that was previously the side or bottom of the boulder, or that the samples do not represent glacially transported boulders, but are rather rock fall from upslope surfaces. We invoke this latter process to explain the very young exposure ages of Skåla samples SK05-6, SK05-10, and SK05-11 (Table 2.1). Unlike Blåhø and Elgåhogna, the lower slopes of Skåla are steep, and thus rock fall from above is not unexpected.

Anomalously old samples (e.g. BL05-4, BL05-7, SK05-9, EL05-17) are interpreted to contain inherited nuclides from previous exposure. If boulders were formed via plucking from the underlying bedrock, it is possible in some cases that the bedrock was not eroded sufficiently, resulting in inherited nuclides from previous exposure, increasing the apparent exposure age of the sample. Although there is the risk of sampling a previously exposed surface, it is only a one in six chance for a roughly cubic

boulder, as compared to the five in six chance of sampling an unexposed surface and the greater risk of sampling bedrock with inherited nuclides.

An additional issue for interpreting an exposure age concerns the impact of erosion, which reduces the apparent exposure age if not accounted for. All exposure ages are strictly speaking minimum ages with respect to erosion. In addition, the significance of erosion could vary from sample to sample. Brook et al. (1996) calculated a maximum erosion rate for samples at Skåla by assuming that the oldest sample was at steady state with respect to erosion and production. Applying their calculated maximum erosion rate of 2.4 g cm^{-2} ka^{-1} (~0.92 cm ka^{-1}) increases exposure ages by 8-10% for samples with ages of 10-12 ka, while ages increase by ~17% for LGM age samples. André (2002) reported an independent erosion rate of 0.2 mm ka^{-1} for granitic and metamorphic rocks in Fennoscandia. Applying this erosion rate has little effect (difference <0.5%) on the apparent exposure age. This latter erosion rate is more likely to be closer to the true value because it us unlikely that the Brook et al. (1996) sample was at secular equilibrium. However, the erosion rate of Brook et al. (1996) is from a blockfield surface and this erosion rate may be more representative of erosion rates at high elevations, such as in a summit blockfield.
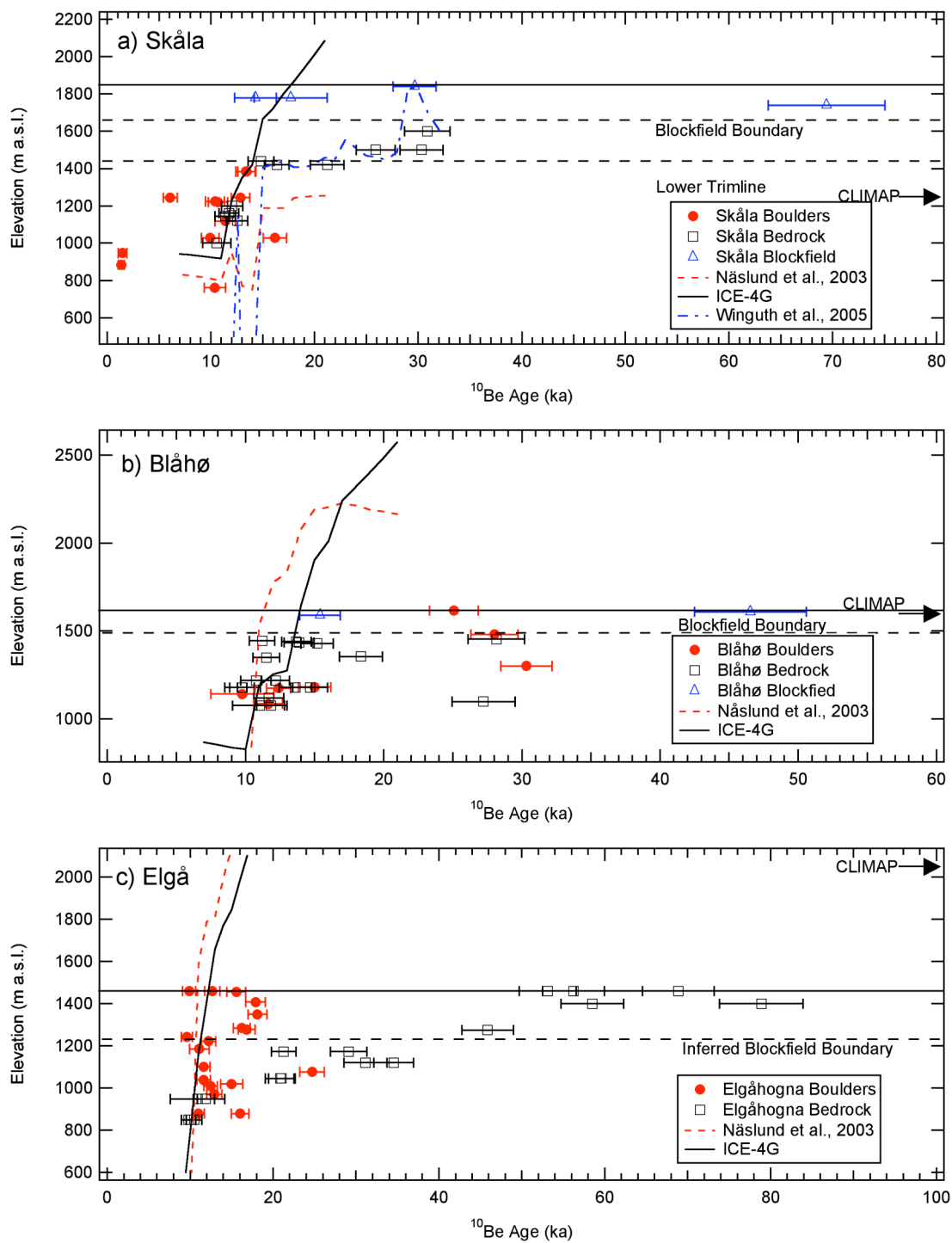
Figure 2.5

Figure 2.5. Elevation vs. [10]Be Age for each site in this study: a) Skåla, b) Blåhø, and c) Elgåhogna. Solid circles are boulder exposure ages, open squares are bedrock exposure ages, and open triangles are blockfield exposure ages. Solid line indicates summit elevation; dashed lines indicate blockfield boundary or trimline elevation. Bedrock and blockfield exposure ages are from Brook et al. (1996, in prep) and Linge et al. (2006). Also shown are ice sheet elevations from time dependent ice sheet models of the FIS of Näslund et al. (2003) and Peltier (1994) at Skåla, Blåhø, and Elgåhogna, as well as the Nordfjord flowline model of Winguth et al. (2005) at Skåla only. LGM FIS elevations for each site based on the CLIMAP (Hughes, 1981) maximum model are also shown.

The above calculation assumes long-term constant erosion. There is a possibility that erosion has been by episodic slab release or spalling of boulder surfaces. Although this is unlikely given the lithologies and sampled boulders, it could dramatically lower apparent exposure ages. Slab release or spalling was avoided by selecting samples that showed weathered surfaces and/or had lichen cover, both of which are indicative of stable surfaces that have experienced no erosion or gradual erosion. One exception may be the summit samples from Elgåhogna, where an age pattern observed in the boulder ages is similar to that observed in bedrock from the same locality, accelerated erosion at the summit has been inferred to explain the age distribution of the bedrock samples (Linge et al., 2006).

Exposure ages may also be affected by attenuation of cosmic rays by snow, decreasing the apparent exposure age. Although sampling was carried out in an effort to avoid possible snow cover by choosing the largest boulders present, the possibility remains that snow may have covered boulder surfaces at least seasonally. Long-term snow depth information is not available for any of the areas sampled in this study. A theoretical calculation of the impact of seasonal (4 months) snow cover 1 m thick (based

on Norsk Meteorologisk Institutt snow records from sites nearby) reduces surface production rates by ca. 12%.

2.5.3 FIS Geometry from Exposure Ages

Our exposure ages from glacially transported boulders provide constraints on past ice sheet elevation and its temporal evolution. Results from all three areas show major changes in the surface elevation of FIS between ca. 9-12 ka. Older ages are distributed differently at the three sites, due to differences in elevation.

In this section we also use ice sheet elevations inferred from exposure ages and compare them to ice sheet elevations predicted by several recent time dependent models of the FIS: a 3-D thermo-mechanical ice sheet model forced by the GRIP ice core record (Näslund et al., 2003), a high resolution 2-D flow line model for Nordfjord forced by a modified GISP2 ice core record (Winguth et al., 2005), and an inversion of crustal isostatic rebound (Peltier, 1994; herein referred to as ICE-4G). Other models of the LGM FIS include that based on the distribution of blockfield weathering zones (Nesje et al., 1988; Nesje and Dahl, 1990), the CLIMAP maximum model, which uses the distribution of moraines and glacial features to model ice flow and height (Hughes, 1981), the model of Boulton et al. (1985), which is constructed in a similar fashion to the CLIMAP model, but accounts for soft sediment deformation, and the 3-D thermo-mechanical model of Siegert and Dowdeswell (2004), controlled by AGCM temperature and precipitation results. The latter three models are not be used in the current comparison either because they are not time dependent, or the raw output data were not available.

Skåla

Boulder ages at Skåla generally increase with elevation, if the three young and one old outlier are assumed to be a result of the processes explained above. Boulder ages also agree fairly well with ages from bedrock surfaces at Skåla (Brook et al., 1996, in prep; Figure 2.5a). Boulder and bedrock exposure age agreement implies sufficient erosion to reset the "cosmogenic clock" of the bedrock surfaces. Based on our results for these lower elevation samples, the FIS surface at Skåla was at ~1384 m at ~13.4 ka. As mentioned above, no boulders were observed above this elevation; however, bedrock samples indicate the LGM ice surface was at least 1400 m (Brook et al., 1996, in prep). Samples SK05-1 and SK05-2 at 1384 m rest just below the "lower trimline" of McCarroll and Nesje (1993), confirming the bedrock results of Brook et al. (1996). It is likely then that the LGM FIS was at the lower trimline (1440 m) and the blockfield boundary (1560 m) may be the result of an earlier thicker ice advance (>30 ka), but other scenarios cannot be ruled out due the lack of boulders. Therefore, the blockfield boundary at Skåla appears to be a glacial trimline, but from a pre-LGM ice sheet. The data indicate that FIS thinning following the LGM was very gradual (~6.1 m/kyr) until ~13.4 ka. After 13.4 ka, the FIS at Skåla appears to have lost surface elevation very rapidly. Our record of deglaciation continues until ~10 ka, when the FIS surface elevation dropped below 760 m (Figure 2.5a).

Results from three of the ice sheet models discussed above are shown in Figure 2.5a for Skåla. The model of Näslund et al. (2003) predicts lower FIS elevations than our data suggest for the LGM and has deglaciation occurring earlier than the data indicate.

The higher resolution flowline model of Winguth et al. (2005) does the best job at predicting ice elevation at the LGM; however, their model also predicts major thinning occurring before our results indicate. ICE-4G, on the other hand, agrees well with our data during major thinning; however, ICE-4G appears to over predict LGM ice sheet elevation by ~600 m. These are surprising results, as it might be expected that a 2-D flow line model with high-resolution bed topography, and forcing by a local climate proxy would result in the most accurate deglacial chronology. In the Winguth et al. (2005) model, ice surface elevation matches our chronology if deglaciation in the model is delayed by ~4 kyr, implying that the response time of the ice sheet to climate changes may be too rapid or the climate changes forcing the model may be occurring too early. Differences between our results and the model of Näslund et al. (2003) may result from calving of the ice sheet in Nordfjord as the ice margin began to retreat. The model of Näslund et al. (2003) does not account for sea level during glacial times; flooding of Nordfjord might have led to accelerated disintegration of the FIS, which may not have occurred if sea level was adjusted to deglacial levels. In addition, both Winguth et al. (2005) and Näslund et al. (2003) use Greenland ice core records (modified GISP2 in Winguth et al. (2005), GRIP in Näslund et al. (2003)) as the climate forcing mechanism in their models. This may suggest that the use of Greenland climate proxy records as ice sheet forcing may not be valid for the FIS.

An alternative interpretation of our results, as suggested by the ice sheet models of Winguth et al. (2005) and Näslund et al. (2003), is that following the LGM, at ~14.5 ka, there was a major thinning of the FIS at Skåla, possibly during the Bølling-Allerod,

followed by a thickening of the FIS at ~12 ka, likely during the Younger Dryas (YD).

Our boulder results may be recording this behavior and we present this as alternative to

the above scenario. The interpretation rests on the data from boulder SK05-9 (1028 m,

16.2±1.0 ka), interpreted above as an outlier due to previous exposure. This boulder

could have been deposited by an initial thinning due to retreat of the FIS to 1028 m

(Figure 2.5a). Sometime after 16.2 ka, the FIS may have readvanced, increasing the

surface elevation at Skåla to ~1400 m, possibly during the Younger Dryas, which is

recorded as an increase in ice rafted detritus in the Norwegian Sea, as well as moraines in

southern Norway (Mangerud, 2004). If boulders are perfect recorders of ice surface

elevation, during the readvance previously deposited boulders could have been

transported away from the region. Thinning would then lead to the deposition of the

boulders sampled in our study and record the subsequent thinning of the FIS, likely

following the Younger Dryas.

Blåhø

Boulders from elevations lower than ~1300 m at Blåhø show reasonable

agreement with bedrock exposure ages (Brook et al., in prep), suggesting that sufficient

erosion of bedrock surfaces occurred to reset the "cosmogenic clock" in these lower

samples (Figure 2.5b). We infer from our boulder results that the LGM FIS was at ~1600

m or higher based on BL05-6 (1617 m, 25.1 ka). Both BL05-7 (28.0 ka) at 1481 m and

BL05-4 (30.3 ka) at 1302 m likely contain a component of inherited nuclides. We

conclude this because bedrock surfaces at similar elevations have lower exposure ages,

and we would expect the lower exposure ages to be seen in boulders rather than bedrock,

thus bedrock ages at this elevation represent deglaciation timing. The thinning history at Blåhø is very similar to that observed at Skåla. Thinning began at ~25 ka at 1617 m, proceeded slowly to ~1450 m by ~14 ka based on the large number of bedrock samples at this elevation. Following ~14 ka, thinning was very rapid and the FIS was below ~1000 m by 10 ka. It is interesting to note that the maximum height of the FIS occurs at ~25 ka, rather than the accepted 19-21 ka of the LGM. However, (Baumann et al., 1995) argued that ice rafted detritus data indicate that the FIS reached its maximum extent in the western part of the ice sheet prior to the accepted LGM at ~25 ka.

Above the blockfield boundary, bedrock exposure ages are both older and younger than the one sampled boulder, which has an exposure age of ~25 ka. Only a single boulder was located in the small summit blockfield; however, we are confident that it is an erratic based on its non-local lithology as well as well developed rounding of the boulder, compared to the angular blockfield (Figure 2.4). We interpret the boulder age to represent deglaciation of the summit blockfield to preserve old blockfield surfaces, thus preservation of blockfield surfaces beneath cold based ice is inferred, as well as processes creating blockfield surfaces with young exposure ages, such as slab break off or rotation of blocks to explain a young blockfield age in Figure 2.5.

Ice sheet elevations predicted for Blåhø by ICE-4G and Näslund et al. (2003) are shown in Figure 2.5b. Our results place the LGM FIS at an elevation of ~1600 m. It is clear that both models predict much higher FIS elevation at the LGM, ICE-4G by ~800 m and Näslund et al. (2003) by ~600 m. During thinning of the FIS following the LGM,

both models predict ice elevations consistent with our data, especially during the later stage of thinning ca. 10 ka.

Elgåhogna

At all elevations greater than 1000 m at Elgåhogna, boulder exposure ages are much lower than bedrock exposure ages, except for EL05-17 (1077 m, 24.7 ka) (Figure 2.5c). Differences between bedrock and boulder exposure ages are discussed further below. The age distribution of the seven uppermost samples is curious because the upper three samples have lower ages than four samples immediately below. We suggest two possible interpretations.

First, it is possible that the three summit boulders are experiencing rapid and uneven erosion. Rapid erosion, such as spalling, will remove a large quantity of accumulated nuclides over a very short time. Additionally, spalling of boulders surfaces will not be uniform from boulder to boulder. This interpretation is supported by observations of a similar pattern of ages (younger at summit) in bedrock samples from the same elevation. Under this interpretation the LGM FIS was likely above the Elgåhogna summit and did not thin to 1400 m until ~17.3 ka. Thinning proceeded until it slowed between ~16 and ~11.1 ka, after which the FIS thinned rapidly. By ~10 ka, the FIS was at or below 880 m.

An alternative interpretation of the boulder exposure ages from Elgåhogna is that the four samples found just below the summit, EL05-5, EL05-9, EL05-11, and EL05-12 were deposited by an initial deglaciation at ~17.3 ka (Figure 2.5c). The FIS then increased in elevation from ~1250 m to the summit or above at ~13 ka, possibly during

the Younger Dryas. However, sea level records for this period of time show continuous increase in relative sea level due primarily to melting of the LGM northern hemisphere ice sheets arguing against a major thickening of the FIS near its center, on the other hand, it is unlikely that sea level records (Fairbanks, 1989; Bard et al., 1990; Bard et al., 1996; Hanebuth et al., 2000) have sufficient resolution to discern a thickening of the FIS considering that the entire FIS/Kara-Barents Ice Sheet complex may have contributed only 4.6 m of sea level change during MWP-1a (Peltier, 2004), which is the approximate resolution of the sea level records (Fairbanks, 1989). Final thinning of the FIS at Elgåhogna may have commenced at ~11.3 ka and the FIS was at 880 m by ~10 ka. We inferred a similar behavior of the FIS at Skåla based in part on ice sheet models that predict a readvance of the ice sheet during this time, whereas at Elgåhogna, the same models do not predict readvance. Regardless of the two scenarios presented, it is likely that the LGM FIS was at least at 1460 m, and likely greater, based on the presence of younger than LGM aged boulders resting on the summit.

The two available time dependent ice sheet elevation predictions (ICE-4G; Näslund et al., 2003) for Elgåhogna are shown in Figure 2.5c. Predicted LGM elevations from both models are greater than 2000 m. Unfortunately, we are unable to place exact constraints on the LGM thickness of the FIS here, except that is was above 1460 m. Both models predict the rapid thinning of the FIS beginning ~11.3 ka.

2.5.4 The LGM FIS in southern Norway

From our exposure age results and previous bedrock exposure ages we can begin

to understand the geometry of the FIS in southern Norway at the LGM (Figure 2.6). At

Skåla, the LGM ice surface was likely at ~1440 m, corresponding with the mapped lower

trimline. At Blåhø, the ice surface was at approximately 1600 m, possibly greater. At

Elgåhogna, the ice surface was at least 1460 m, likely much greater. The blockfield

boundary at Skåla may have been created during an earlier thicker ice advance based on

bedrock exposure ages, but other scenarios cannot be ruled out. At Blåhø and Elgåhogna,

we infer that ice was covering the blockfields that therefore must have survived beneath

low erosive ice (see discussion below). Inland summits with blockfields at other locations

may also have been experiencing similar conditions, casting doubt on ice limits

reconstructed from blockfield distributions.

Until the release of ICE-4G, the CLIMAP ice sheet reconstruction was used in

many AGCMs for the LGM, whereas ICE-4G is now widely used. Our results indicate

large discrepancies between predicted elevations from ICE-4G and elevation estimates

based on exposure ages. Differences between ICE-4G and our results are 650, 1420, and

up to 1085 m thicker for Skåla, Blåhø, and Elgåhogna respectively. At least for the FIS,

CLIMAP may be an alternative in AGCMs as the differences between CLIMAP

elevations and elevations from exposure ages are much smaller (Figure 2.6). The use of a

higher elevation ice sheet (ICE-4G) may produce increases in temperature downwind of

an ice sheet as compared to the use of a thinner ice sheet (CLIMAP) (Shinn and Barron,

1989; Ramstein and Joussaume, 1995; Felzer et al., 1996; Barron and Pollard, 2002;

Pollard and Barron, 2003). The use of correct ice sheet heights in AGCMs has important

implications regarding our understanding of glacial climate, especially in regions

downwind of the major LGM ice sheets.
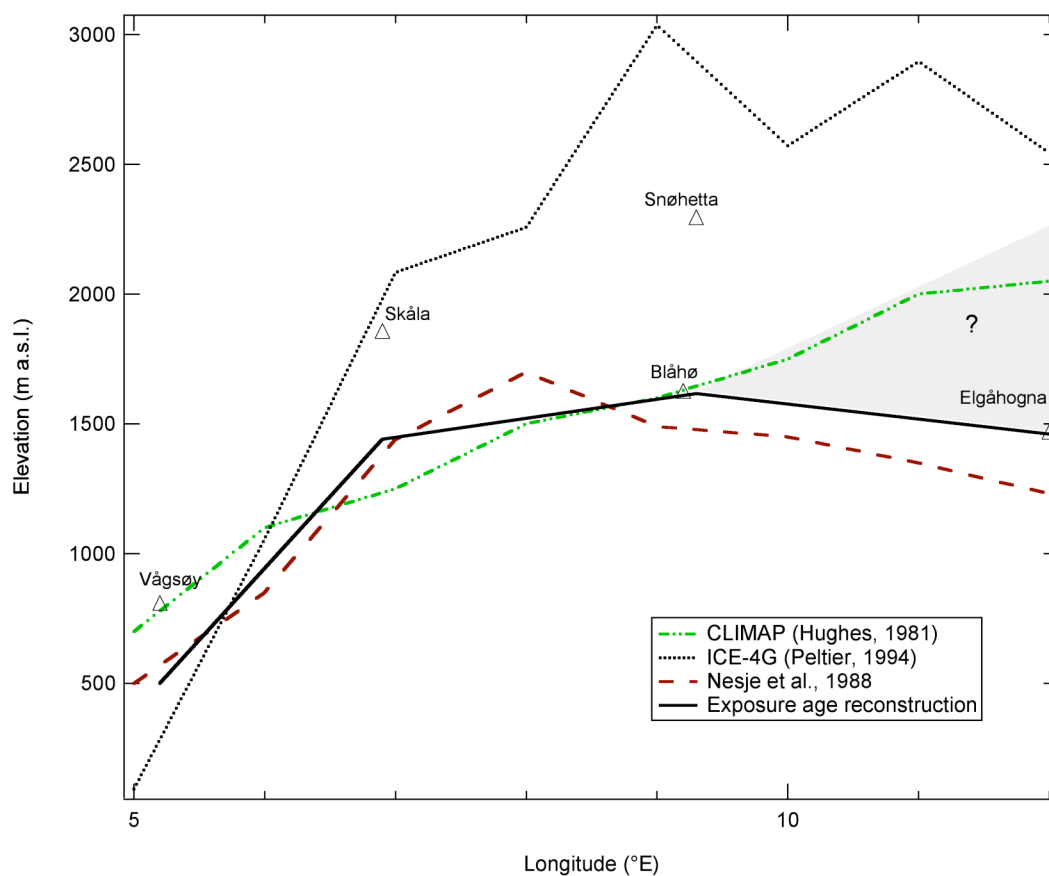
Figure 2.6. Profile of the LGM FIS at 62°N as reconstructed by CLIMAP (Hughes, 1981), ICE-4G (Peltier, 1994), the blockfield weathering hypothesis (Nesje et al., 1988), and a reconstruction based on our exposure ages. Our reconstruction at Elgåhogna is a minimum and the FIS was likely at higher elevations shown in the gray shading.

2.5.5 Preservation of Previously Exposed Surfaces

Fabel et al. (2002) and Stroeven et al. (2002) have shown that tor surfaces in

northern Sweden experienced multiple episodes of ice sheet cover by cold-based ice.

Other studies suggest cold-based ice in other areas of the LGM FIS (e.g. Kleman, 1994; Kleman and Hätterstrand, 1999). Our study suggests that the Elgåhogna and Blåhø regions of the FIS were also cold-based and previously exposed blockfield and bedrock surfaces are preserved. Progressive and large divergence in exposure age between boulder samples and bedrock samples at Elgåhogna is definitive evidence for preservation of bedrock surfaces under cold-based ice (Figure 2.7). This progressive difference in exposure age is presumably due to varying amounts of subglacial erosion with elevation, implying partial resetting of the "cosmogenic clock" at intermediate elevations. Figure 2.7 shows the elevation range where we infer partial resetting of bedrock samples. A possible interpretation combining the exposure ages with geomorphic features above the blockfield boundary is that bedrock samples have experienced minimal or zero resetting, and the "blockfield boundary" represents a subglacial thermal boundary between frozen bed non-erosive ice above and a wet-bed region that was progressively more erosive with increasing ice thickness. It is expected that as ice thickens, the bed should approach the pressure melting point, increasing the erosive capacity of the ice due to inception of basal sliding (Patterson, 1994).
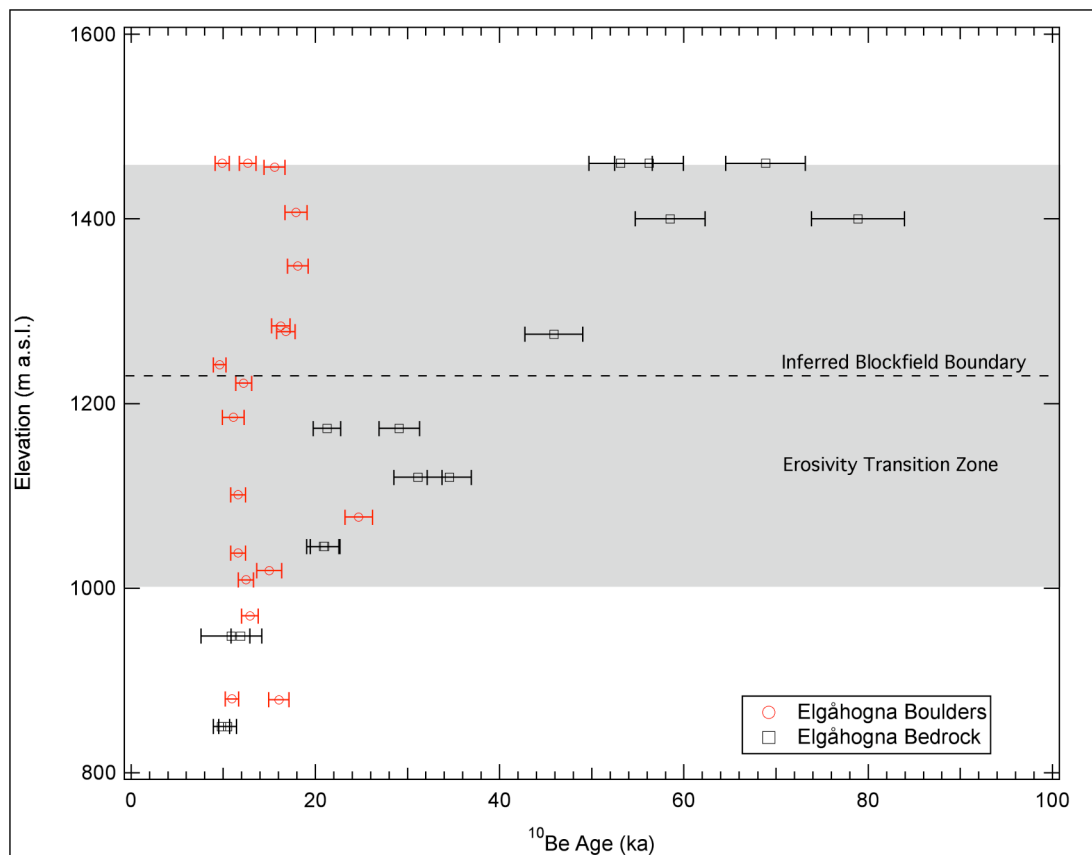
Figure 2.7. Boulder exposure ages and bedrock exposure ages from Elgåhogna show the progressive divergence between boulder and bedrock exposure ages with increasing elevation. Boulder and bedrock exposure ages are equivalent at low elevations where sufficient erosion is inferred to have reset the "cosmogenic clock". Gray shaded area shows the regions where we interpret partial resetting of bedrock surfaces.

Evidence from Elgåhogna resolves a long-standing debate over the age of blockfields, which is related to controversies about the thickness of the FIS. The apparent trend in the lower limit of blockfields mapped by Nesje et al. (1988), previously interpreted as the LGM ice sheet limit in eastern Norway (LGM limit at ~1200 m at Elgåhogna), appears to represent a subglacial thermal boundary, which controls subglacial erosive capacity, rather than the elevation of the LGM FIS (Figure 2.7). Our

exposure ages allow the conclusion that blockfields are old features that have survived beneath low erosive through at least one glacial cycle. In many cases, it is likely that blockfields have survived multiple periods of exposure and burial in order to accumulate bedrock [10]Be concentrations measured from Elgåhogna. Linge et al. (2006, their figure 4) show that blockfields may be as old as ~1 Ma, depending of the glaciation history used in their model, but certainly older than ~250 ka.

2.6 Conclusions

Beryllium-10 exposure ages of glacially transported boulders from three regions of southern Norway provide constraints on the elevation of the FIS at and since the LGM. Ice was likely at ~1440 m during the LGM at Skåla, while further inland at Blåhø, LGM ice was at 1500-1600 m. At Elgåhogna, ice was at least at 1460 m and likely greater. After the LGM, exposure ages show that the FIS rapidly lost elevation following the Younger Dryas at all locations.

Our study provides a comparison of boulder exposure ages with ice sheet elevations predicted by several recent ice sheet models for the last glacial cycle. In general, ice sheet elevations during deglaciations predicted by ICE-4G and Näslund et al. (2003) are similar to constraints based on exposure ages for Blåhø and Elgåhogna. At Skåla, a flow line model (Winguth et al., 2005), and one thermo-mechanical ice sheet model (Näslund et al., 2003) underestimate the elevation of the FIS during deglaciation, while the ICE-4G isostatic inversion model seems to more accurately reconstruct ice sheet elevations. However, the same isostatic inversion model overestimates ice elevation

during the LGM at Blåhø and Skåla. At Elgåhogna we are unable to provide comparisons

with the reconstructions of the models due to the absence of boulders with LGM

exposure ages. At all locations, the difference between ice sheet elevations predicted by

the CLIMAP Maximum model and our results is much less than with the ICE-4G model.

This suggests that CLIMAP may be a better FIS model for use in AGCMs.

We also conclude that regions of the FIS experienced frozen bed conditions,

inferred from the survival of ^{10}Be in bedrock and blockfield surfaces covered by ice at the

LGM. This supports other studies of the FIS basal thermal regime that have found

evidence for survival of previously exposed bedrock surfaces (Fabel et al., 2002;

Stroeven et al., 2002). At Elgåhogna, not only do we recognize that areas of the FIS were

frozen to its bed, we also observe evidence for a shift from frozen bed low erosive

conditions under thinner summit-covering ice to melting bed more erosive conditions

under thicker valley-filling ice. Results from Elgåhogna resolve a long-standing debate

regarding the age of blockfields. Our results suggest that blockfields are long-lived

features (Roaldset et al., 1982; Rea et al., 1996; Linge et al., 2006) that have survived

under ice through at least one glacial cycle, rather than representing the upper limit of an

ice surface (Nesje et al., 1988; Linge et al., 2006).

Future work in Norway will yield more information about the elevation evolution

of the FIS during the transition from the glacial conditions of the LGM to the interglacial

conditions of the Holocene. Constraints on the thickness of the FIS may allow for

estimates of ice volume change during periods of major sea level change, and thus

improving our understanding of the contributions to sea level change from individual ice

sheets may finally be better understood. Additionally, reanalysis of bedrock from

Elgåhogna for ^{10}Be and ^{26}Al in combination with our boulder exposure ages may allow

for the calculation of total glacial erosion following the method of Fabel et al. (2004).

2.7 Acknowledgments

2.8 References

Ackert, R. P., Barclay, D. J., Borns Jr., H. W., Calkin, P. E., Kurz, M. D., Fastook, J. L. and Steig, E. J., 1999. Measurements of past ice sheet elevations in interior West Antarctica. Science, 286: 276-280.

André, M.-F., 2002. Rates of postglacial rock weathering on glacially scoured outcrops (Abisko-Riksgränsen area, 68°N). Geografiska Annaler, 84A: 139-150.

Bard, E., Hamelin, B., Arnold, M., Montaggioni, L., Cabioch, G., Faure, G. and Rougerie, F., 1996. Deglacial sea-level record from Tahiti corals and the timing of global meltwater discharge. Nature, 382: 241-244.

Bard, E., Hamelin, B. and Fairbanks, R., 1990. U-Th ages obtained by mass spectrometry in corals from Barbados sea level during the past 130,000 years. Nature, 346: 456-458.

Barron, E. and Pollard, D., 2002. High-Resolution Climate Simulations of Oxygen Isotope Stage 3 in Europe. Quaternary Research, 58: 296-309.

Baumann, K.-H., Lackscewitz, K. S., Mangerud, J., Spielhagen, R. F., Wolf-Welling, T. C. W., Henrich, R. and Kassens, H., 1995. Reflection of Scandinavian Ice Sheet Fluctuations in Norwegian Sea Sediments during the Past 150,000 Years. Quaternary Research, 43: 185-197.

Bierman, P. R., Marsella, K. A., Patterson, C., Davis, P. T. and Caffee, M., 1999. Mid-Pleistocene minimum-age limits for pre-Wisconsinan glacial surfaces in

southwestern Minnesota and southern Baffin Island: a multiple nuclide approach. Geomorphology, 27: 25-39.

Boulton, G. S., Smith, G. D., Jones, A. S. and Newsome, J., 1985. Glacial geology and glaciology of the last mid-latitude ice sheets. J. geol. Soc. London, 142: 447-474.

Briner, J. P., Miller, G. H., Davis, P. T., Bierman, P. R. and Caffee, M., 2003. Last Glacial Maximum ice sheet dynamics in Arctic Canada inferred from young erratics perched on ancient tors. Quaternary Science Reviews, 22: 437-444.

Briner, J. P., Miller, G. H., Davis, P. T. and Finkel, R., 2006. Cosmogenic radionuclides from fiord landscapes support differential erosion by overriding ice sheets. GSA Bulletin, 118: 406-420.

Briner, J. P. and Swanson, T. W., 1998. Using inherited cosmogenic ^{36}Cl to constrain glacial erosion rates of the Cordilleran ice sheet. Geology, 26: 3-6.

Brook, E. J., Nesje, A., Lehman, S. J., Raisbeck, G. M. and Yiou, F., 1996. Cosmogenic nuclide exposure ages along a vertical transect in western Norway: Implications for the height of the Fennoscandian ice sheet. Geology, 24: 207-210.

Brown, E. T., Brook, E. J., Raisbeck, G. M., Yiou, F. and Kurz, M. D., 1992. Effective attenuation lengths of cosmic rays producing ^{10}Be and ^{26}Al in quartz: Implications for exposure age dating. Geophys. Res. Lett., 19: 369-372.

Carlson, A., Clark, P. U., Raisbeck, G. M. and Brook, E. J., in prep. Rapid Holocene Delgaciation of the Labrador Sector of the Laurentide Ice Sheet. Journal of Climate,

Clark, P. U., McCabe, A. M., Mix, A. C. and Weaver, A. J., 2004. Rapid Rise of Sea Level 19,000 Years Age and Its Global Implications. Science, 304: 1141-1144.

Clark, P. U. and Mix, A. C., 2002. Ice sheets and sea level of the Last Glacial Maximum. Quaternary Science Reviews, 21: 1-7.

Colgan, P. M., Bierman, P. R., Mickelson, D. M. and Caffee, M., 2002. Variation in glacial erosion near the southern margin of the Laurentide Ice Sheet, south-central Wisconsin, USA: Implication for cosmogenic dating of glacial terrains. Geological Society of America Bulletin, 114: 1581-1591.

Dahl, R., 1966a. Block fields and other weathering forms in the Narvik Mountains. Geografiska Annaler, 48A: 224-227.

Dahl, R., 1966b. Block fields, weathering pits and tor-like forms in the Narvik Mountains, Nordland, Norway. Geografiska Annaler, 48A: 55-85.

Dunne, J., Elmore, D. and Muzikar, P., 1999. Scaling factors for the rates of production of cosmogenic nuclides for geometric shielding and attenuation at depth on sloped surfaces. Geomorphology, 27: 3-11.

Fabel, D., Harbor, J., Dahms, D., James, A., Elmore, D., Horn, L., Daley, K. and Steele, C., 2004. Spatial Patterns of Glacial Erosion at a Valley Scale Derived From Terrestrial Cosmogenic ^{10}Be and ^{26}Al Concentrations in Rock. Annals of the Association of American Geographers, 94: 241-255.

Fabel, D., Stroeven, A. P., Harbor, J., Kleman, J., Elmore, D. and Fink, D., 2002. Landscape preservation under Fennoscandian ice sheets determined from in situ produced 10Be and 26Al. Earth and Planetary Science Letters, 201: 397-406.

Fairbanks, R., 1989. A 17,000-year glacio-eustatic sea level record: influence of glacial melting rates on the Younger Dryas even and deep ocean circulation. Nature, 342: 637-642.

Fairbridge, R. W., 1968. The Encyclopedia of Geomorphology. Fairbridge, R. W., Encyclopedia of the Earth Sciences Series. Reinhold Book Corporation, New York,

Felzer, B., Oglesby, R. J., Webb III, T. and Hyman, D. E., 1996. Sensitivity of a general circulation model to changes in northern hemisphere ice sheets. Journal of Geophysical Research, 10: 19,077-19,092.

Follestad, B., 1990. Block fields, ice-flow directions and the Pleistocene ice sheet in Nordmøre and Romsdal, West Norway. Norsk Geologisk Tidsskrift, 70: 27-33.

Goehring, B. M., 2006. [10]Be Exposure ages of erratic boulders in southern Norway and implications for the history of the Fennoscandian Ice Sheet. MS, Oregon State University, Corvallis, OR.

Gosse, J. C., Evenson, E. B., Klein, J., Lawn, B. and Middleton, R., 1995a. Precise cosmogenic [10]Be measurements in western North America: Support for a global Younger Dryas cooling event. Geology, 23: 877-880.

Gosse, J. C., Klein, J., Evenson, E. B., Lawn, B. and Middelton, R., 1995b. Beryllium-10 Dating of the Duration and Retreat of the Last Pinedale Glacial Sequence. Science, 268: 1329-1333.

Hanebuth, T., Stattegger, K. and Grootes, P. M., 2000. Rapid Flooding of the Sunda Shelf: A Late-Glacial Sea-Level Record. Science, 288: 1033-1035.

Hughes, T. J., 1981. Numerical reconstruction of paleo-ice sheets. Denton, G. H. and Hughes, T. J., The last great ice sheets. John Wiley & Sons, New York, 221-261.

Kageyama, M., Valdes, P. J., Ramstein, G., Hewitt, C. and Wyputta, U., 1999. Northern Hemisphere Storm Tracks in Present Day and Last Glacial Maximum Climate Simulations: A Comparison of the European PMIP Models. Journal of Climate, 12: 742-760.

Kleman, J., 1994. Preservation of landforms under ice sheet and ice caps. Geomorphology, 9: 19-32.

Kleman, J. and Borgstrom, I., 1990. The Boulder Fields of Mt. Fulufjallet, West-Central Sweden -Late Weichselian Boulder Blankets and Interstadial Periglacial Phenomena. Geografiska Annaler, 72A: 63-78.

Lal, D., 1991. Cosmic ray labeling of erosion surfaces: *in situ* nuclide production rates and erosion models. Earth and Planetary Science Letters, 104: 424-439.

Licciardi, J. M., 2000. Alpine glacier and pluvial lake records of late Pleistocene climate variability in the western United States. PhD, Oregon State Univ., Corvallis, Oregon.

Linge, H., Brook, E. J., Nesje, A., Raisbeck, G., Yiou, F. and Clark, H., 2006. *In situ* [10]Be exposure ages from southeastern Norway: implications for the geometry of the Weichselian Scandinavian ice sheet. Quaternary Science Reviews, 25: 1097-1109.

Lundberg, J. and Ford, D. C., 1994. Late Pleistocene sea level change in the Bahamas from mass spectrometric U-series dating of submerged speleothem. Quaternary Science Reviews, 13: 1-14.

Manabe, S. and Broccoli, A. J., 1985. The Influence of Continental Ice Sheets on Climate of an Ice Age. Journal of Geophysical Research, 90: 2167-2190.

Mangerud, J., 1991. The Scandinavian Ice Sheet through the last interglacial/glacial cycle. Frenzel, B., Klimageschichtliche Probleme der letzen 130,000 Jahre. G. Fischer, Stuttgart, New York, 307-330.

Mangerud, J., 2004. Ice sheet limits in Norway and on the Norwegian continental shelf. Ehlers, J. and Gibbard, P. L., Quaternary Glaciations-Extent and Chronology. Elsevier, Amsterdam, 271-295.

Marquette, G. C., Gray, J. T., Gosse, J. C., Corchesne, F., Stokli, L., Macpherson, G. and Finkel, R., 2004. Felsenmeer persistence under non-erosive ice in the Torngat and Kaumajet mountains, Quebec and Labrador, as determined by soil weathering and cosmogenic nuclide exposure dating. Can. J. Earth Sci., 41: 19-38.

McCarroll, D. and Nesje, A., 1993. The vertical extent of ice sheets in Nordfjord, western Norway: measuring degree of rock surface weathering. Boreas, 22: 255-265.

Middleton, R., Brown, L., Dezfouly-Arjomandy, B. and Klein, J., 1993. On [10]Be standards and the half-life of [10]Be. Nuclear Instruments and Methods in Physics Research B, 82: 399-403.

Morén, L. and Påsse, T., 2001. Climate and shoreline in Sweden during Weichsel and the next 150,000 years. SKB Technical Report 01-19. Swedish Nuclear Fue and Waste Management Co., Stockholm. 67.

Nesje, A., Anda, E., Rye, N., Lien, R., Hole, P. A. and Blikra, L. H., 1987. The vertical extent of the Late Weichselian ice sheet in the Nordfjord-Møre area, western Norway. Norsk Geologisk Tidsskrift, 67: 125-141.

Nesje, A. and Dahl, S. O., 1990. Autochthonous block fields in southern Norway: implications for the geometry, thickness, and isostatic loading of the Late Weichselian ice sheet. Journal of Quaternary Science, 5: 225-234.

Nesje, A. and Dahl, S. O., 1992. Equilibrium-line altitude depressions of reconstructed Younger Dryas and Holocene glaciers in Fosdalen, inner Nordfjord, western Norway. Norsk Geologisk Tidsskrift, 72: 209-216.

Nesje, A., Dahl, S. O., Anda, E. and Rye, N., 1988. Block fields in southern Norway: Significance for the Late Weichselian ice sheet. Norsk Geologisk Tidsskrift, 68: 149-169.

Nesje, A., McCarroll, D. and Dahl, S. O., 1994. Degree of rock surface weathering as an indicator of ice-sheet thickness along an east-west transect across southern Norway. Journal of Quaternary Science, 9: 337-347.

Nishiizumi, K., Winterer, E. L., Kohl, C. P., Klein, J., Middelton, R., Lal, D. and Arnold, J. R., 1989. Cosmic Ray Production Rates of [10]Be and [26]Al in Quartz From Glacially Polished Rocks. Journal of Geophysical Research, 94: 17,907-17,915.

Näslund, J. O., Rodhe, L., Fastook, J. L. and Holmlund, P., 2003. New ways of studying ice sheet flow directions and glacial erosion by computer modeling-examples from Fennoscandia. Quaternary Science Reviews, 22: 245-258.

Patterson, W. S. B., 1994. The Physics of Glaciers. Butterworth-Heinemann, Oxford.

Peltier, W. R., 1994. Ice Age Paleotopography. Science, 265: 195-201.

Peltier, W. R., 2004. Global Glacial Isostasy and the Surface of the Ice-Age Earth: The ICE-5G (VM2) Model and GRACE. Annu. Rev. Earth Planet Sci., 32: 111-149.

Pigati, J. S. and Lifton, N. A., 2004. Geomagnetic effects on time-integrated cosmogenic nuclide production with emphasis on in situ ^{14}C and [10]Be. Earth and Planetary Science Letters, 226: 193-205.

Pollard, D. and Barron, E., 2003. Causes of model-data discrepancies in European climate during oxygen isotope stage 3 with insights from the last glacial maximum. Quaternary Research, 59: 108-113.

Putkonen, J. and Swanson, T., 2003. Accuracy of cosmogenic ages for moraines. Quaternary Research, 59: 255-261.

Påsse, T., 1997. A mathematical model of past, present and future shore level displacement in Fennoscandia. SKB Technical Report 97-28. Swedish Nuclear Fuel and Waste Management Co., Stockholm. 55.

Raisbeck, G. M., Yiou, F., Bourlés, D., Brown, E., Deboffle, D., Jouhanneau, P., Lestringuez, J. and Zhou, Z. Q., 1994. The AMS facility at Gif-sur-Yvette: progress, perturbations and projects. Nuclear Instruments and Methods in Physics Research B, 92: 43-46.

Ramstein, G. and Joussaume, S., 1995. Sensitivity experiments to sea surface temperatures, sea-ice extent and ice-sheet reconstruction, for the Last Glacial Maximum. Annals of Glaciology, 21: 343-347.

Rea, B. R., Whalley, W. B., Rainey, M. M. and Gordon, J. E., 1996. Blockfields, old or new? Evidence and implication from some plateaus in northern Norway. Geomorphology, 15: 109-121.

Rinterknecht, V. R., Clark, P. U., Raisbeck, G. M., Yiou, F., Bitinas, A., Brook, E. J., Marks, L., Zelčs, V., Lunkka, J.-P., Pavlovskaya, I. E., Piotrowski, J. A. and Raukas, A., 2006. The Last Deglaciation of the Southeastern Sector of the Scandinavian Ice Sheet. Science, 311: 1449-1452.

Rinterknecht, V. R., Clark, P. U., Raisbeck, G. M., Yiou, F., Brook, E. J., Tschudi, S. and Lunkka, J.-P., 2004. Cosmogenic [10]Be dating of the Salpausselkä I Moraine in southwestern Finland. Quaternary Science Reviews, 23: 2283-2289.

Roaldset, E., Pettersen, E., Longva, O. and Mangerud, J., 1982. Remnants of preglacial weathering in western Norway. Norsk Geologisk Tidsskrift, 62: 169-178.

Sejrup, H. P., Larsen, E., Landvik, J., King, E. L., Haflidason, H. and Nesje, A., 2000. Quaternary glaciations in southern Fennoscandia: evidence from southern Norway and the northern North Sea region. Quaternary Science Reviews, 19: 667-685.

Shackleton, N. J., 1987. Oxygen isotopes, ice volume and sea level. Quaternary Science Reviews, 6: 183-190.

Shinn, R. A. and Barron, E. J., 1989. Climate Sensitivity to Continental Ice Sheet Size and Configuration. Journal of Climate, 2: 1517-1537.

Siegert, M. J. and Dowdeswell, J. A., 2004. Numerical reconstructions of the Eurasian Ice Sheet and climate during the Late Weichselian. Quaternary Science Reviews, 23: 1273-1283.

Sigmond, E. M. O., Gustavson, M. and Roberts, D., 1984. Berggrunnskart over Norge-M. 1:1 million. Norges geologiske undersøkelse,

Steig, E. J., Wolfe, A. P. and Miller, G. H., 1998. Wisconsinan refugia and the glacial history of eastern Baffin Island, Arctic Canada: Coupled evidence from cosmogenic isotopes and lake sediments. Geology, 26: 835-838.

Stone, J. O., 2000. Air pressure and cosmogenic isotope production. Journal of Geophysical Research, 105: 23,753-23,759.

Stone, J. O., Balco, G. A., Sugden, D. E., Caffee, M. W., Sass III, L. C., Cowdery, S. G. and Siddoway, C., 2003. Holocene Deglaciation of Marie Byrd Land, West Antarctica. Science, 299: 99-102.

Stone, J. O., Ballantyne, C. K. and Fifield, L. K., 1998. Exposure dating and validation of periglacial weathering limits, northwest Scotland. Geology, 26: 587-590.

Stroeven, A. P., Fabel, D., Hättestrand, C. and Harbor, J., 2002. A relict landscape in the centre of Fennoscandian glaciation: cosmogenic radionuclide evidence of tors preserved through multiple glacial cycles. Geomorphology, 44: 145-154.

Winguth, C., Mickelson, D. M., Larsen, E., Darter, J. R., Moeller, C. A. and Stalsburg, K., 2005. Thickness evolution of the Scandinavian Ice Sheet during the Late Weichselian in Nordfjord, western Norway: evidence from ice-flow modeling. Boreas, 34: 176-185.

Yokoyama, Y., Esat, T. M., Lambeck, K. and Fifield, L. K., 2000. Last Ice Age millennial scale climate changes recorded in Huon Peninsula corals. Radiocarbon, 42: 383-401.

Chapter 3

Conclusions

3.1 Conclusions

Beryllium-10 exposure ages of glacially transported boulders from three regions of southern Norway provide constraints on the elevation of the FIS at and since the LGM. Ice was likely at ~1440 m during the LGM at Skåla, while further inland at Blåhø, LGM ice was at 1500-1600 m. At Elgåhogna, ice was at least at 1460 m and likely greater. After the LGM, exposure ages show that the FIS rapidly lost elevation following the Younger Dryas at all locations.

Our study provides a comparison of boulder exposure ages with ice sheet elevations predicted by several recent ice sheet models for the last glacial cycle. In general, ice sheet elevations during deglaciations predicted by ICE-4G and Näslund et al. (2003) are similar to constraints based on exposure ages for Blåhø and Elgåhogna. At Skåla, a flow line model (Winguth et al., 2005), and one thermo-mechanical ice sheet model (Näslund et al., 2003) underestimate the elevation of the FIS during deglaciation, while the ICE-4G isostatic inversion model seems to more accurately reconstruct ice sheet elevations. However, the same isostatic inversion model overestimates ice elevation during the LGM at Blåhø and Skåla. At Elgåhogna we are unable to provide comparisons with the reconstructions of the models due to the absence of boulders with LGM exposure ages. At all locations, the difference between ice sheet elevations predicted by

the CLIMAP Maximum model and our results is much less than with the ICE-4G model. This suggests that CLIMAP may be a better FIS model for use in AGCMs.

We also conclude that regions of the FIS experienced frozen bed conditions, inferred from the survival of [10]Be in bedrock and blockfield surfaces covered by ice at the LGM. This supports other studies of the FIS basal thermal regime that have found evidence for survival of previously exposed bedrock surfaces (Fabel et al., 2002; Stroeven et al., 2002). At Elgåhogna, in eastern Norway, not only do we recognize that areas of the FIS were frozen to its bed, we also observe a shift from frozen bed low erosive conditions under thinner summit covering ice to melting bed more erosive conditions under thicker valley filling ice. Results from Elgåhogna resolve a long-standing debate regarding the age of blockfields. Our results suggest that blockfields are long-lived features (Roaldset et al., 1982; Rea et al., 1996; Linge et al., 2006) that have survived under ice through at least one glacial cycle, rather than representing the upper limit of an ice surface (Nesje et al., 1988; Linge et al., 2006).

Bibliography

Ackert, R. P., Barclay, D. J., Borns Jr., H. W., Calkin, P. E., Kurz, M. D., Fastook, J. L. and Steig, E. J., 1999. Measurements of past ice sheet elevations in interior West Antarctica. Science, 286: 276-280.

André, M.-F., 2002. Rates of postglacial rock weathering on glacially scoured outcrops (Abisko-Riksgränsen area, 68°N). Geografiska Annaler, 84A: 139-150.

Bard, E., Hamelin, B., Arnold, M., Montaggioni, L., Cabioch, G., Faure, G. and Rougerie, F., 1996. Deglacial sea-level record from Tahiti corals and the timing of global meltwater discharge. Nature, 382: 241-244.

Bard, E., Hamelin, B. and Fairbanks, R., 1990. U-Th ages obtained by mass spectrometry in corals from Barbados sea level during the past 130,000 years. Nature, 346: 456-458.

Barron, E. and Pollard, D., 2002. High-Resolution Climate Simulations of Oxygen Isotope Stage 3 in Europe. Quaternary Research, 58: 296-309.

Baumann, K.-H., Lackscewitz, K. S., Mangerud, J., Spielhagen, R. F., Wolf-Welling, T. C. W., Henrich, R. and Kassens, H., 1995. Reflection of Scandinavian Ice Sheet Fluctuations in Norwegian Sea Sediments during the Past 150,000 Years. Quaternary Research, 43: 185-197.

Bierman, P. R., Marsella, K. A., Patterson, C., Davis, P. T. and Caffee, M., 1999. Mid-Pleistocene minimum-age limits for pre-Wisconsinan glacial surfaces in southwestern Minnesota and southern Baffin Island: a multiple nuclide approach. Geomorphology, 27: 25-39.

Boulton, G. S., Smith, G. D., Jones, A. S. and Newsome, J., 1985. Glacial geology and glaciology of the last mid-latitude ice sheets. J. geol. Soc. London, 142: 447-474.

Briner, J. P., Miller, G. H., Davis, P. T., Bierman, P. R. and Caffee, M., 2003. Last Glacial Maximum ice sheet dynamics in Arctic Canada inferred from young erratics perched on ancient tors. Quaternary Science Reviews, 22: 437-444.

Briner, J. P., Miller, G. H., Davis, P. T. and Finkel, R., 2006. Cosmogenic radionuclides from fiord landscapes support differential erosion by overriding ice sheets. GSA Bulletin, 118: 406-420.

Briner, J. P. and Swanson, T. W., 1998. Using inherited cosmogenic 36Cl to constrain glacial erosion rates of the Cordilleran ice sheet. Geology, 26: 3-6.

Brook, E. J., Nesje, A., Lehman, S. J., Raisbeck, G. M. and Yiou, F., 1996. Cosmogenic nuclide exposure ages along a vertical transect in western Norway: Implications for the height of the Fennoscandian ice sheet. Geology, 24: 207-210.

Brown, E. T., Brook, E. J., Raisbeck, G. M., Yiou, F. and Kurz, M. D., 1992. Effective attenuation lengths of cosmic rays producing ^{10}Be and ^{26}Al in quartz: Implications for exposure age dating. Geophys. Res. Lett., 19: 369-372.

Carlson, A., Clark, P. U., Raisbeck, G. M. and Brook, E. J., in prep. Rapid Holocene Deglaciation of the Labrador Sector of the Laurentide Ice Sheet. Journal of Climate,

Clark, P. U., McCabe, A. M., Mix, A. C. and Weaver, A. J., 2004. Rapid Rise of Sea Level 19,000 Years Age and Its Global Implications. Science, 304: 1141-1144.

Clark, P. U. and Mix, A. C., 2002. Ice sheets and sea level of the Last Glacial Maximum. Quaternary Science Reviews, 21: 1-7.

Colgan, P. M., Bierman, P. R., Mickelson, D. M. and Caffee, M., 2002. Variation in glacial erosion near the southern margin of the Laurentide Ice Sheet, south-central Wisconsin, USA: Implication for cosmogenic dating of glacial terrains. Geological Society of America Bulletin, 114: 1581-1591.

Dahl, R., 1966a. Block fields and other weathering forms in the Narvik Mountains. Geografiska Annaler, 48A: 224-227.

Dahl, R., 1966b. Block fields, weathering pits and tor-like forms in the Narvik Mountains, Nordland, Norway. Geografiska Annaler, 48A: 55-85.

Dunne, J., Elmore, D. and Muzikar, P., 1999. Scaling factors for the rates of production of cosmogenic nuclides for geometric shielding and attenuation at depth on sloped surfaces. Geomorphology, 27: 3-11.

Fabel, D., Harbor, J., Dahms, D., James, A., Elmore, D., Horn, L., Daley, K. and Steele, C., 2004. Spatial Patterns of Glacial Erosion at a Valley Scale Derived From Terrestrial Cosmogenic ^{10}Be and ^{26}Al Concentrations in Rock. Annals of the Association of American Geographers, 94: 241-255.

Fabel, D., Stroeven, A. P., Harbor, J., Kleman, J., Elmore, D. and Fink, D., 2002. Landscape preservation under Fennoscandian ice sheets determined from in situ produced 10Be and 26Al. Earth and Planetary Science Letters, 201: 397-406.

Fairbanks, R., 1989. A 17,000-year glacio-eustatic sea level record: influence of glacial melting rates on the Younger Dryas even and deep ocean circulation. Nature, 342: 637-642.

Fairbridge, R. W., 1968. The Encyclopedia of Geomorphology. Fairbridge, R. W., Encyclopedia of the Earth Sciences Series. Reinhold Book Corporation, New York,

Felzer, B., Oglesby, R. J., Webb III, T. and Hyman, D. E., 1996. Sensitivity of a general circulation model to changes in northern hemisphere ice sheets. Journal of Geophysical Research, 10: 19,077-19,092.

Follestad, B., 1990. Block fields, ice-flow directions and the Pleistocene ice sheet in Nordmøre and Romsdal, West Norway. Norsk Geologisk Tidsskrift, 70: 27-33.

Goehring, B. M., 2006. ^{10}Be Exposure ages of erratic boulders in southern Norway and implications for the history of the Fennoscandian Ice Sheet. MS, Oregon State University, Corvallis, OR.

Hanebuth, T., Stattegger, K. and Grootes, P. M., 2000. Rapid Flooding of the Sunda Shelf: A Late-Glacial Sea-Level Record. Science, 288: 1033-1035.

Hughes, T. J., 1981. Numerical reconstruction of paleo-ice sheets. Denton, G. H. and Hughes, T. J., The last great ice sheets. John Wiley & Sons, New York, 221-261.

Kageyama, M., Valdes, P. J., Ramstein, G., Hewitt, C. and Wyputta, U., 1999. Northern Hemisphere Storm Tracks in Present Day and Last Glacial Maximum Climate Simulations: A Comparison of the European PMIP Models. Journal of Climate, 12: 742-760.

Kleman, J., 1994. Preservation of landforms under ice sheet and ice caps. Geomorphology, 9: 19-32.

Kleman, J. and Borgstrom, I., 1990. The Boulder Fields of Mt. Fulufjallet, West-Central Sweden -Late Weichselian Boulder Blankets and Interstadial Periglacial Phenomena. Geografiska Annaler, 72A: 63-78.

Lal, D., 1991. Cosmic ray labeling of erosion surfaces: *in situ* nuclide production rates and erosion models. Earth and Planetary Science Letters, 104: 424-439.

Licciardi, J. M., 2000. Alpine glacier and pluvial lake records of late Pleistocene climate variability in the western United States. PhD, Oregon State Univ., Corvallis, Oregon.

Linge, H., Brook, E. J., Nesje, A., Raisbeck, G., Yiou, F. and Clark, H., 2006. *In situ* [10]Be exposure ages from southeastern Norway: implications for the geometry of the Weichselian Scandinavian ice sheet. Quaternary Science Reviews, 25: 1097-1109.

Lundberg, J. and Ford, D. C., 1994. Late Pleistocene sea level change in the Bahamas from mass spectrometric U-series dating of submerged speleothem. Quaternary Science Reviews, 13: 1-14.

Manabe, S. and Broccoli, A. J., 1985. The Influence of Continental Ice Sheets on Climate of an Ice Age. Journal of Geophysical Research, 90: 2167-2190.

Mangerud, J., 1991. The Scandinavian Ice Sheet through the last interglacial/glacial cycle. Frenzel, B., Klimageschichtliche Probleme der letzen 130,000 Jahre. G. Fischer, Stuttgart, New York, 307-330.

Mangerud, J., 2004. Ice sheet limits in Norway and on the Norwegian continental shelf. Ehlers, J. and Gibbard, P. L., Quaternary Glaciations-Extent and Chronology. Elsevier, Amsterdam, 271-295.

Marquette, G. C., Gray, J. T., Gosse, J. C., Corchesne, F., Stokli, L., Macpherson, G. and Finkel, R., 2004. Felsenmeer persistence under non-erosive ice in the Torngat and Kaumajet mountains, Quebec and Labrador, as determined by soil weathering and cosmogenic nuclide exposure dating. Can. J. Earth Sci., 41: 19-38.

McCarroll, D. and Nesje, A., 1993. The vertical extent of ice sheets in Nordfjord, western Norway: measuring degree of rock surface weathering. Boreas, 22: 255-265.

Middleton, R., Brown, L., Dezfouly-Arjomandy, B. and Klein, J., 1993. On [10]Be standards and the half-life of [10]Be. Nuclear Instruments and Methods in Physics Research B, 82: 399-403.

Morén, L. and Påsse, T., 2001. Climate and shoreline in Sweden during Weichsel and the next 150,000 years. SKB Technical Report 01-19. Swedish Nuclear Fuel and Waste Management Co., Stockholm. 67.

Nesje, A., Anda, E., Rye, N., Lien, R., Hole, P. A. and Blikra, L. H., 1987. The vertical extent of the Late Weichselian ice sheet in the Nordfjord-Møre area, western Norway. Norsk Geologisk Tidsskrift, 67: 125-141.

Nesje, A. and Dahl, S. O., 1990. Autochthonous block fields in southern Norway: implications for the geometry, thickness, and isostatic loading of the Late Weichselian ice sheet. Journal of Quaternary Science, 5: 225-234.

Nesje, A. and Dahl, S. O., 1992. Equilibrium-line altitude depressions of reconstructed Younger Dryas and Holocene glaciers in Fosdalen, inner Nordfjord, western Norway. Norsk Geologisk Tidsskrift, 72: 209-216.

Nesje, A., Dahl, S. O., Anda, E. and Rye, N., 1988. Block fields in southern Norway: Significance for the Late Weichselian ice sheet. Norsk Geologisk Tidsskrift, 68: 149-169.

Nesje, A., McCarroll, D. and Dahl, S. O., 1994. Degree of rock surface weathering as an indicator of ice-sheet thickness along an east-west transect across southern Norway. Journal of Quaternary Science, 9: 337-347.

Nishiizumi, K., Winterer, E. L., Kohl, C. P., Klein, J., Middelton, R., Lal, D. and Arnold, J. R., 1989. Cosmic Ray Production Rates of ^{10}Be and ^{26}Al in Quartz From Glacially Polished Rocks. Journal of Geophysical Research, 94: 17,907-17,915.

Näslund, J. O., Rodhe, L., Fastook, J. L. and Holmlund, P., 2003. New ways of studying ice sheet flow directions and glacial erosion by computer modeling-examples from Fennoscandia. Quaternary Science Reviews, 22: 245-258.

Patterson, W. S. B., 1994. The Physics of Glaciers. Butterworth-Heinemann, Oxford.

Peltier, W. R., 1994. Ice Age Paleotopography. Science, 265: 195-201.

Peltier, W. R., 2004. Global Glacial Isostasy and the Surface of the Ice-Age Earth: The ICE-5G (VM2) Model and GRACE. Annu. Rev. Earth Planet Sci., 32: 111-149.

Pigati, J. S. and Lifton, N. A., 2004. Geomagnetic effects on time-integrated cosmogenic nuclide production with emphasis on in situ ^{14}C and ^{10}Be. Earth and Planetary Science Letters, 226: 193-205.

Pollard, D. and Barron, E., 2003. Causes of model-data discrepancies in European climate during oxygen isotope stage 3 with insights from the last glacial maximum. Quaternary Research, 59: 108-113.

Påsse, T., 1997. A mathematical model of past, present and future shore level displacement in Fennoscandia. SKB Technical Report 97-28. Swedish Nuclear Fuel and Waste Management Co., Stockholm. 55.

Raisbeck, G. M., Yiou, F., Bourlés, D., Brown, E., Deboffle, D., Jouhanneau, P., Lestringuez, J. and Zhou, Z. Q., 1994. The AMS facility at Gif-sur-Yvette: progress, perturbations and projects. Nuclear Instruments and Methods in Physics Research B, 92: 43-46.

Ramstein, G. and Joussaume, S., 1995. Sensitivity experiments to sea surface temperatures, sea-ice extent and ice-sheet reconstruction, for the Last Glacial Maximum. Annals of Glaciology, 21: 343-347.

Rea, B. R., Whalley, W. B., Rainey, M. M. and Gordon, J. E., 1996. Blockfields, old or new? Evidence and implication from some plateaus in northern Norway. Geomorphology, 15: 109-121.

Rinterknecht, V. R., Clark, P. U., Raisbeck, G. M., Yiou, F., Bitinas, A., Brook, E. J., Marks, L., Zelčs, V., Lunkka, J.-P., Pavlovskaya, I. E., Piotrowski, J. A. and Raukas, A., 2006. The Last Deglaciation of the Southeastern Sector of the Scandinavian Ice Sheet. Science, 311: 1449-1452.

Rinterknecht, V. R., Clark, P. U., Raisbeck, G. M., Yiou, F., Brook, E. J., Tschudi, S. and Lunkka, J.-P., 2004. Cosmogenic ^{10}Be dating of the Salpausselkä I Moraine in southwestern Finland. Quaternary Science Reviews, 23: 2283-2289.

Roaldset, E., Pettersen, E., Longva, O. and Mangerud, J., 1982. Remnants of preglacial weathering in western Norway. Norsk Geologisk Tidsskrift, 62: 169-178.

Sejrup, H. P., Larsen, E., Landvik, J., King, E. L., Haflidason, H. and Nesje, A., 2000. Quaternary glaciations in southern Fennoscandia: evidence from southern Norway and the northern North Sea region. Quaternary Science Reviews, 19: 667-685.

Shackleton, N. J., 1987. Oxygen isotopes, ice volume and sea level. Quaternary Science Reviews, 6: 183-190.

Shinn, R. A. and Barron, E. J., 1989. Climate Sensitivity to Continental Ice Sheet Size and Configuration. Journal of Climate, 2: 1517-1537.

Siegert, M. J. and Dowdeswell, J. A., 2004. Numerical reconstructions of the Eurasian Ice Sheet and climate during the Late Weichselian. Quaternary Science Reviews, 23: 1273-1283.

Sigmond, E. M. O., Gustavson, M. and Roberts, D., 1984. Berggrunnskart over Norge-M. 1:1 million. Norges geologiske undersøkelse,

Steig, E. J., Wolfe, A. P. and Miller, G. H., 1998. Wisconsinan refugia and the glacial history of eastern Baffin Island, Arctic Canada: Coupled evidence from cosmogenic isotopes and lake sediments. Geology, 26: 835-838.

Stone, J. O., 2000. Air pressure and cosmogenic isotope production. Journal of Geophysical Research, 105: 23,753-23,759.

Stone, J. O., Balco, G. A., Sugden, D. E., Caffee, M. W., Sass III, L. C., Cowdery, S. G. and Siddoway, C., 2003. Holocene Deglaciation of Marie Byrd Land, West Antarctica. Science, 299: 99-102.

Stone, J. O., Ballantyne, C. K. and Fifield, L. K., 1998. Exposure dating and validation of periglacial weathering limits, northwest Scotland. Geology, 26: 587-590.

Stroeven, A. P., Fabel, D., Hättestrand, C. and Harbor, J., 2002. A relict landscape in the centre of Fennoscandian glaciation: cosmogenic radionuclide evidence of tors preserved through multiple glacial cycles. Geomorphology, 44: 145-154.

Winguth, C., Mickelson, D. M., Larsen, E., Darter, J. R., Moeller, C. A. and Stalsburg, K., 2005. Thickness evolution of the Scandinavian Ice Sheet during the Late Weichselian in Nordfjord, western Norway: evidence from ice-flow modeling. Boreas, 34: 176-185.

Yokoyama, Y., Esat, T. M., Lambeck, K. and Fifield, L. K., 2000. Last Ice Age millennial scale climate changes recorded in Huon Peninsula corals. Radiocarbon, 42: 383-401.

Appendix A

Sample Photos and Descriptions

Figure A1a. Samples collected at Skåla. Locations are in UTM coordinates, NAD 1983 Datum.

	SK05-1 Augen feldspar gneiss sitting on bedrock ridge in center of bowl, possibly a cirque. Approx. 2m x 1.3 m x 1.0 m Elevation 1384 m Location: 32V 0392155, 6860486
	SK05-2 Augen feldspar gneiss sitting on same bedrock ridge as SK05-1, taken ~15 m away from SK05-1. Elevation 1384 m Location: 32V 0392155, 6860486
	SK05-3 Augen gneiss boulder sitting on bedrock ridge between cirque and Lotvatnet valley. Many boulders near here. Approx. 0.4 m x 0.5 m x 0.5 m. Elevation: 1223 m Location: 32V 039401, 6860519

Figure A1b.

	SK05-4 Rounded augen gneiss boulder resting ~10 m south of SK05-3, slightly lower elevation. Approx. 1 m x 0.8 m x 1.2 m. Elevation: 1220 m Location: 32V 0391401, 6860519
	SK05-5 Boulder resting on slope below lower trimline. Local augen gneiss lithology that shown differential weathering. Other large boulders near by, but show less weathering. Approx. 4 m x 3 m x 3 m. Elevation: 1244 m Location: 32V 0391592, 6861164
	SK05-6 Located approx. 10 m from SK05-5. Similar lithology, but weathering is not nearly a developed. Slightly smaller than SK05-5. Elevation: 1244 m Location: 32V 0391592, 6861164

Figure A1c.

	SK05-7 Augen gneiss boulder resting on bedrock just outside of the cirque. Approx. 2 m x 2 m x 3 m. Elevation: 1118 m Location: 32V 0391279, 661089
	SK05-8 Very large boulder comprised of augen gneiss, possibly resting on a recessional moraine. May be partially buried. Approx. 4 m x 2 m x 2 m. Elevation: 1028 m Location: 32V 0391093, 6861287
	SK05-9 Rests slightly uphill of SK05-8. Lithology is augen gneiss. Elevation: 1028 m Location: 32V 0391093, 6861287

Figure A1d.

	SK05-10 Very large (4 m x 3.3 m x 3.2 m) boulder resting on till like material. May still be on moraine material. Elevation: 947 m Location: 32V 0390913, 6861445
	SK05-11 Rounded large boulder (3.8 m x 1.8 m x 2.4 m) resting on terrace in adjacent valley to Lovatnet. Lithology is augen gneiss. Elevation: 885 m Location: 32V 0390890, 6861837
	SK05-12 Boulder resting on terrace like feature below lateral moraines. Lithology is augen gneiss. Approx. 2 m x 2 m x 1.5 m. Elevation: 761 Location: 32V 0390826, 6862218

Figure A2a. Samples collected at Blåhø. Locations are in UTM coordinates, NAD 1983 Datum.

	BL05-1 Perched quartz-mica schist resting on bedrock. Bedrock shows striations, striations strike in direction of major ice flow. Elevation: 1142 m Location: 32V 0507526, 6862590
	BL05-2 Quartz-mica schist boulder resting on striated bedrock. Boulder is approx. 2 m x 1 m x 1 m. Elevation: 1086 m Location: 32V 0507257, 6862805
	BL05-3 Quartz rich schist/gneiss resting on bedrock will till nearby. Located on north of small lake. Approx. 1 m x 1 m x 1 m. Elevation: 1176 m Location: 32V 0509027, 6863545

Figure A2b.
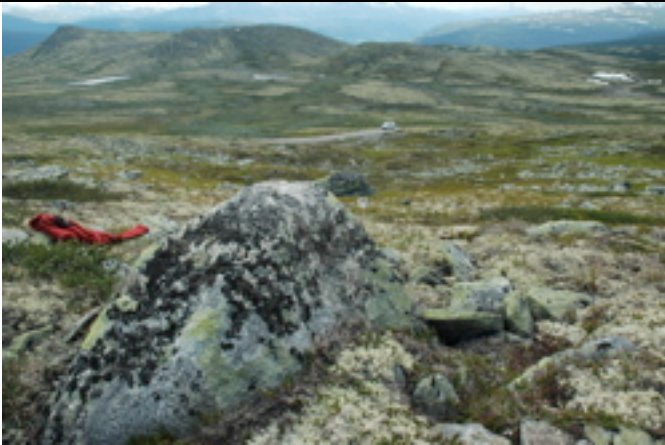
	BL05-4 Granitic gneiss resting on till like material. Boulder rests on small hill north of road. Approx. 1 m^3. Elevation: 1302 m Location: 32V 0511019, 6863452
	BL05-5 Granitic migmatite gneiss resting on bedrock. Approx. 150 m north of road. Boulder is approx. 1 m x 1 m x 0.8 m. Elevation: 1182 m Location: 32V 0508712, 6863371
	BL05-6 Small granitic migmatite gneiss in summit blockfield. No other boulders were found in blockfield, but lithology is clearly not local. Approx. 0.5 m x 0.5 m x 0.5 m. Elevation: 1617 m Location: 32V 0514949, 6862813

Figure A2c.

BL05-7
Quartz-mica schist boulder just below blockfield boundary; rests on angular blocks, which may be blockfield. Approx. 1 m x 0.7 m x 0.5 m.
Elevation: 1481 m
Location: 32V 0513293, 6863393
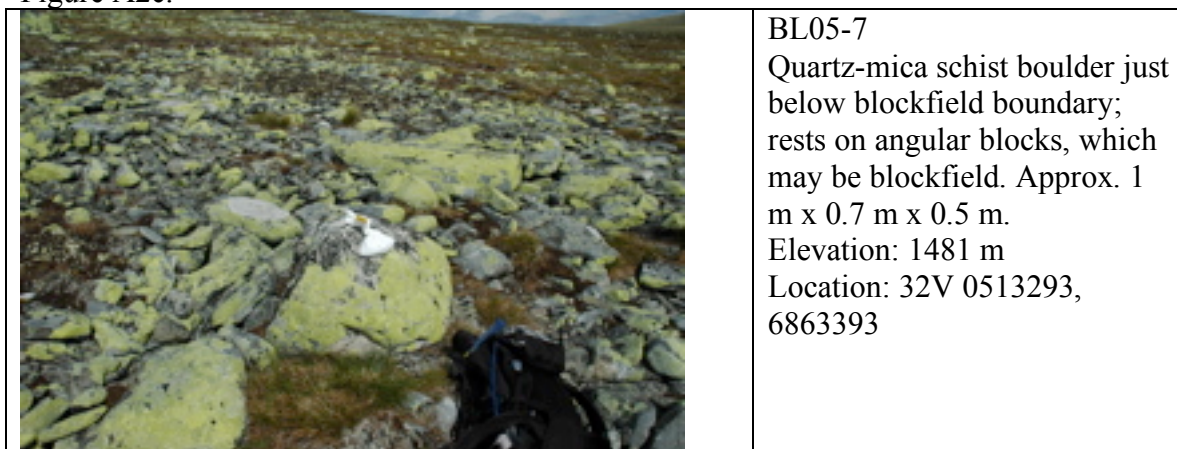
Figure A3a. Samples collected at Elgåhogna. Locations are in UTM coordinates, NAD 1983 Datum.

	EL05-1 Gray meta-sandstone perched on bedrock. Size is approx. 1.7 m x 1.5 m x 1.5 m. Elevation: 879 m Location: 33V 0344140, 6893133
	EL05-2 Pink quartzite boulder resting on till, approx. 1 m^3. Elevation: 970 m Location: 33V 0344591, 6893583
	EL05-3 Large (~2.4 m x 1.8 m x 2 m) arkosic sandstone resting thin cover of debris. Low quartz content. Elevation: 1019 m Location: 33V 0344733, 6893794

Figure A3b.
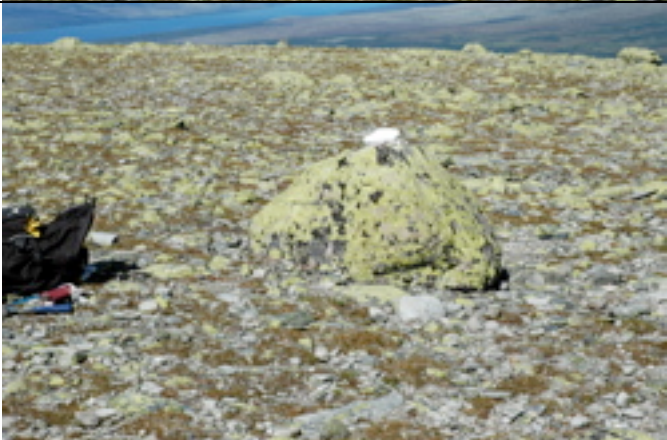
	EL05-4 Arkose sandstone resting on blocky material resembling fractured bedrock. Approx. 2 m x 1.5 m x 1 m. Elevation: 1185 m Location: 33V 0346078, 6893957
	EL05-5 Rounded meta-sandstone boulder resting on loose material. Approx. 1.8 m x 1 m x 0.8 m. Elevation: 1278 m Location: 33V 0346281, 6894608
	EL05-6 Abundant boulders on summit. Rounded meta-sandstone in "blockfield". Approx. 1 m^3. Elevation: 1460 m Location: 33V 0347076, 6894230

Figure A3c.

	EL05-7 Rounded quartz rich meta-sandstone boulder, approx. 0.8 m x 0.7 m x 0.8 m. Sitting on blocky debris. Elevation: 1456 m Location: 33V 0347028, 6894298
	EL05-8 Rounded quartzite south of summit, approx. 1.2 m x 1 m x 0.9 m. Resting on blocky material. Elevation: 1460 m Location: 33V 0347072, 6894177
	EL05-9 Rounded meta-sandstone boulder sitting on till like material, may be in blockfield. Approx. 2 m x 1.6 m x 1 m. Elevation: 1407 m Location: 33V 0347062, 6893859

Figure A3d.

	EL05-11 Quartz rich meta-sandstone, rounded, loose blocks surround boulder. Approx. 2 m x 1.8 m x 1 m. Elevation: 1349 m Location: 33V 0346838, 6893660
	EL05-12 Rounded, gray meta-sandstone perched on blocky material. Approx. 1.6 m x 1.3 m x 1.7 m. Elevation: 1284 m Location: 33V 0346331, 6893605
	EL05-13 Sub-rounded quartzite boulder sitting in blockfield like material. Approx. 1 m x 1.6 m x 1.3 m. Elevation: 1242 m Location: 33V 0345955, 6893676

Figure A3e.

	EL05-14 Subrounded gray quartzite boulder resting in blockfield. Approx. 1 m^3. Elevation: 1222 m Location: 33V 0345930, 6893671
	EL05-15 Slightly pinkish meta-sandstone resting on boulder mantled slope. Approx. 2 m x 1.3 m x 1.4 m. Elevation: 1009 m Location: 33V 0344274, 6893659
	EL05-16 Large tabular boulder resting on bedrock. Lithology is meta-sandstone, some feldspar, approx. 2.3 m x 2 m x 1.1 m. Elevation: 1038 m Location: 33V 0344378, 6894212

Figure A3f.

	EL05-17 Rounded meta-sandstone resting on loose blocky debris. Approx. 2 m x 1.2 m x 1.1 m. Elevation: 1077 m Location: 33V 0344630, 6894483
	EL05-18 Rounded pink quartzite resting on gray quartzite bedrock. Boulder shows signs of some spalling. Approx. 1.3 m x 1 m x 1 m. Elevation: 1101 m Location: 33V 0344708, 6894364
	EL05-19 Gray meta-sandstone located ~100 m from EL05-1. Boulder rests on bedrock, slightly rounded. Approx. 2 m x 1.7 m x 1.6 m. Elevation: 880 m Location: 33V 0344174, 6893087

Appendix B

Data Tables

Table B1. Major ion concentration of bulk clean quartz. Inductively Coupled Plasma-Optical Emission Spectrometry (ICP-OES) measurements were made on aliquots of pure quartz sample. This was done to check quartz purity. If concentrations were > 500 ppm, quartz was leached an additional 24-48 hrs. Aliquots of ~0.1 g quartz were used for these measurements. See Appendix C for full preparation and measurement procedures.

Sample	Mass Quartz (g)	Mass Solution (g)	Dilution Factor	Al (ppm)	Fe (ppm)	Ti (ppm)	Ca (ppm)	K (ppm)	Na (ppm)	Mg (ppm)
Elgåhogna										
EL05-1	0.207	100.886	487.372	67.11	31.34	28.07	34.80	0	67.06	0
EL05-2	0.117	101.678	869.043	245.07	108.54	126.36	40.41	0	67.87	0
EL05-3	0.135	100.478	744.281	455.05	1093.57	613.06	673.80	0	68.03	0
EL05-4	0.13	100.729	774.838	883.70	1599.58	553.47	33.71	96.39	59.59	0
EL05-5	0.133	100.618	756.526	1017.91	111.74	1.29	32.30	1031.52	129.59	0
EL05-6	0.093	100.102	1076.366	200.31	25.40	6.14	49.08	0	77.82	0
EL05-7	0.171	101.463	593.351	2442.35	261.73	308.90	37.80	2328.78	604.62	0
EL05-8	0.104	101.671	977.606	360.44	116.04	1831.64	32.16	0	93.95	0
EL05-9	0.121	100.479	830.405	167.24	0	20.10	41.27	0	98.49	0
EL05-10	0.102	100.652	986.784	174.36	12550.61	134.50	93.35	0	137.76	0
EL05-11	0.148	101.062	682.851	104.82	21.44	32.71	51.15	0	110.69	0
EL05-12	0.096	101.043	1052.531	1401.34	236.08	44.31	41.68	1102.42	178.51	41.15
EL05-13	0.146	100.088	685.534	218.21	49.22	65.54	39.83	0	63.27	0
EL05-14	0.118	100.728	853.627	150.49	9.65	57.28	64.36	0	171.07	0
EL05-15	0.103	101.942	989.728	73.73	248.32	40.78	48.50	0	124.31	0
EL05-16	0.156	101.412	650.077	102.13	55.19	18.40	30.29	0	64.68	0
EL05-17	0.11	99.612	905.564	1031.53	242.15	30.43	27.71	898.86	151.23	0
EL05-18	0.14	100.249	716.064	347.00	147.65	74.97	31.58	0	61.51	0
EL05-19	0.122	101.172	829.279	79.61	16.25	65.35	45.44	0	80.27	0

Table B1 cont.

Sample	Mass Quartz (g)	Mass Solution (g)	Dilution Factor	Al (ppm)	Fe (ppm)	Ti (ppm)	Ca (ppm)	K (ppm)	Na (ppm)	Mg (ppm)
Skåla										
SK05-1	0.096	99.921	1040.844	38.93	0	0	11.45	0	1.35	0
SK05-2	0.474	100.165	211.319	0	0	0	0	0	12.51	0
SK05-3	0.168	100.565	598.601	66.50	9.46	0	69.62	0	0	0
SK05-4	0.126	100.088	794.349	656.29	0	0	34.32	347.61	68.55	0
SK05-5	0.244	101.283	415.094	97.30	0	0	31.26	0	0	0
SK05-6	0.091	100.825	1107.967	26.81	0	0	40.33	0	0	0
SK05-7	0.151	100.775	667.384	42.51	0	0	23.22	0	0	0
SK05-8	0.204	101.788	498.961	94.60	0	0	13.62	0	0	0
SK05-9	0.219	100.22	457.626	45.58	152.66	33.82	19.31	0	35.05	0
SK05-10	0.359	100.082	278.780	86.34	0.61	0	24.45	0	0	0
SK05-11	0.144	101.041	701.674	767.21	0	0	29.26	548.78	47.08	0
SK05-12	0.104	99.236	954.192	1050.09	256.58	0	155.44	165.84	196.56	0
Blåhø										
BL05-01	0.099	100.179	1011.909	73.57	0	0	5.77	0	57.98	0
BL05-02	0.102	101.253	992.676	49.83	1281.45	38.91	9.53	0	52.91	0
BL05-03	0.118	100.306	850.051	90.62	0	0	47.94	0	58.06	0
BL05-04	0.123	100.416	816.390	33.15	0	0	34.45	0	40.49	0
BL05-05	0.106	100.409	947.255	1384.03	78.15	0	25.58	813.88	324.25	48.22
BL05-06	0.126	100.169	794.992	16647.77	225.94	0	887.05	18311.13	3013.18	0
BL05-07	0.126	101.074	802.175	98.67	0	0	10.43	0	49.57	0

Table B2. Sample information and ^{10}Be data.

a. ^{10}Be/^{9}Be ratios measured at the Tandetron Accelerator Facility at Gif sur-Yvette, France.

b. The number of ^{10}Be atoms and [^{10}Be] are corrected for the error weighted mean of 7 full procedural blanks with and average of 5.45 ± 0.35 x 10^4 atoms.

c. Production rate has been scaled for neutrons and muons independently using Stone (2000) and Nishiizumi et al. (1989) respectively. Production rate shown does not include corrections for topography or sample thickness.

d. Corrections for shielding of cosmic rays by surrounding topography are made following Dunne (1999); samples with no topographic correction have a value of 1. Corrections for sample thickness are made assuming an exponential decrease in production with depth assuming an attenuation length of 155 g/cm^2 and sample density of 2.6 g/cm^3.

Table B2.

Sample	Lat. N DD	Lon. E DD	Alt. m	Weight g qtz	Spike g ^{9}Be	^{10}Be/^{9}Be [a] x 10^{-13}	Counts	^{10}Be[b] 10^6 atoms
Elgåhogna								
EL05-19	62.1374	12.0107	879	49.129	0.251	3.92	484	6.53±0.44
EL05-1	62.1378	12.0100	880	50.478	0.249	3.06	481	5.04±0.34
EL05-2	62.1420	12.0182	970	51.693	0.248	3.93	436	6.47±0.45
EL05-15	62.1426	12.0121	1009	50.395	0.25	3.74	543	6.20±0.41
EL05-3	62.1440	12.0208	1019	13.217	0.249	1.19	186	1.93±0.17
EL05-16	62.1476	12.0136	1038	50.587	0.248	3.65	406	6.00±0.42
EL05-17	62.1501	12.0182	1077	50.502	0.249	6.84	855	11.30±0.69
EL05-18	62.1491	12.0198	1101	50.504	0.242	4.03	422	6.47±0.45
EL05-4	62.1460	12.0464	1185	7.916	0.25	6.56	112	1.04±0.11
EL05-14	62.1434	12.0438	1222	30.252	0.251	2.71	410	4.50±0.32
EL05-13	62.1434	12.0443	1242	49.973	0.248	3.74	413	6.15±0.43
EL05-5	62.1519	12.0497	1278	50.976	0.249	6.13	903	10.20±0.61
EL05-12	62.1429	12.0516	1284	49.447	0.248	5.78	735	9.54±0.59
EL05-11	62.1436	12.0612	1349	55.191	0.248	7.35	765	12.10±0.75
EL05-9	62.1455	12.0653	1407	30.529	0.252	4.21	510	7.04±0.47
EL05-7	62.1494	12.0643	1456	25.053	0.248	3.33	352	5.47±0.40
EL05-8	62.1484	12.0653	1460	51.571	0.249	4.58	284	7.58±0.59
EL05-6	62.1489	12.0653	1460	30.834	0.251	3.45	418	5.74±0.40
Skåla								
SK05-12	61.8770	6.9237	761	26.424	0.252	1.39	135	2.29±0.23
SK05-11	61.8736	6.9252	885	26.392	0.251	0.237	20	0.34±0.08
SK05-10	61.8701	6.9259	947	25.816	0.252	0.254	13	0.37±0.11
SK05-8	61.8687	6.9294	1028	18.887	0.251	1.21	213	1.98±0.17
SK05-9	61.8687	6.9294	1028	44.573	0.246	4.43	416	7.24±0.51
SK05-7	61.8670	6.9330	1118	17.965	0.251	1.4	202	2.29±0.20
SK05-4	61.8619	6.9357	1220	27.838	0.253	2.21	201	3.69±0.32
SK05-3	61.8619	6.9357	1223	25.713	0.246	2.07	195	3.35±0.29
SK05-5	61.8677	6.9389	1244	20.247	0.253	1.94	462	3.23±0.22
SK05-6	61.8677	6.9389	1244	16.293	0.251	0.800	102	1.29±0.14
SK05-1	61.8618	6.9500	1384	25.508	0.251	2.84	365	4.72±0.34
SK05-2	61.8618	6.9500	1384	55.502	0.249	6.22	829	10.30±0.63
Blåhø								
BL05-2	61.89784	9.13809	1086	30.524	0.249	2.32	187	3.81±0.34
BL05-1	61.89590	9.14320	1142	25.034	0.243	1.78	19	2.84±0.67
BL05-3	61.90444	9.17181	1176	30.599	0.25	2.74	433	4.53±0.31
BL05-5	61.90289	9.16580	1182	25.015	0.254	2.59	276	4.35±0.34
BL05-4	61.90355	9.20972	1302	30.477	0.247	6.47	807	10.64±0.65
BL05-7	61.90295	9.25299	1481	37.529	0.251	8.46	856	14.15±0.86
BL05-6	61.89768	9.28446	1617	25.297	0.26	5.51	401	9.53±0.67

Table B2 cont.

Sample	[^{10}Be][b]	Scaling Factors[c]		Production Rate[c]	Shielding[d]	Thickness[d]	^{10}Be Age	Uplift Corrected Age
	10^5 atoms g^{-1} qtz.	Neutrons	Muons	atoms g^{-1} yr^{-1}	Correction		ka	ka
Skåla								
SK05-12	0.87±0.09	2.09	1.44	10.59	0.98	0.98	9.75±0.97	10.37±1.03
SK05-11	0.13±0.03	2.32	1.52	11.74	0.99	0.97	1.32±0.30	1.35±0.31
SK05-10	0.15±0.04	2.45	1.57	12.40	0.98	0.98	1.39±0.39	1.47±0.41
SK05-8	1.05±0.09	2.62	1.63	13.25	0.98	0.98	9.44±0.80	9.93±0.84
SK05-9	1.62±0.11	2.62	1.63	13.25	0.98	0.99	14.44±1.02	16.17±1.14
SK05-7	1.27±0.11	2.82	1.69	14.26	0.99	0.96	10.73±0.93	11.39±0.99
SK05-4	1.33±0.12	3.07	1.77	15.51	0.99	0.98	10.11±0.87	10.69±0.92
SK05-3	1.30±0.11	3.08	1.77	15.56	0.99	0.98	9.85±0.86	10.40±0.91
SK05-5	1.60±0.11	3.13	1.79	15.81	0.98	0.99	11.94±0.81	12.86±0.88
SK05-6	0.79±0.09	3.13	1.79	15.81	0.98	0.99	5.90±0.65	6.08±0.67
SK05-1	1.85±0.13	3.5	1.9	17.67	0.99	0.98	12.36±0.89	13.35±0.97
SK05-2	1.86±0.11	3.5	1.9	17.67	0.99	0.98	12.42±0.75	13.43±0.82
Blåhø								
BL05-2	1.25±0.11	2.75	1.67	13.90	1	0.95	10.82±0.96	11.66±1.03
BL05-1	1.14±0.27	2.88	1.71	14.56	1	0.97	9.21±2.16	9.77±2.29
BL05-3	1.48±0.10	2.96	1.74	14.96	1	0.99	11.44±0.79	12.40±0.86
BL05-5	1.74±0.14	2.98	1.74	15.06	1	0.99	13.38±1.05	15.02±1.17
BL05-4	3.49±0.21	3.28	1.84	16.57	1	0.98	24.69±1.51	30.31±1.85
BL05-7	3.77±0.23	3.78	1.98	19.08	1	0.99	22.92±1.39	28.02±1.70
BL05-6	3.77±0.27	4.2	2.1	21.18	1	0.99	20.61±1.46	25.08±1.77
Elgåhogna								
EL05-19	1.33±0.09	2.31	1.52	11.69	1	0.96	13.57±0.92	16.04±1.08
EL05-1	1.00±0.07	2.31	1.52	11.69	1	0.97	10.08±0.68	10.95±0.74
EL05-2	1.25±0.09	2.5	1.58	12.65	1	0.98	11.55±0.80	12.91±0.89
EL05-15	1.23±0.08	2.58	1.61	13.05	1	0.96	11.24±0.74	12.46±0.82
EL05-3	1.46±0.13	2.6	1.62	13.15	1	0.98	12.97±1.16	15.00±1.34
EL05-16	1.19±0.08	2.64	1.63	13.35	1	0.96	10.63±0.75	11.62±0.82
EL05-17	2.25±0.14	2.73	1.66	13.80	1	0.99	18.88±1.14	24.71±1.49
EL05-18	1.28±0.09	2.78	1.68	14.05	1	0.98	10.64±0.74	11.61±0.81
EL05-4	1.32±0.14	2.98	1.74	15.06	1	0.98	10.24±1.09	11.09±1.18
EL05-14	1.49±0.11	3.07	1.77	15.51	1	0.99	11.11±0.78	12.21±0.86
EL05-13	1.23±0.09	3.12	1.79	15.76	1	0.99	9.02±0.63	9.61±0.67
EL05-5	1.99±0.12	3.22	1.82	16.26	1	0.99	14.16±0.85	16.82±1.01
EL05-12	1.93±0.12	3.23	1.82	16.31	1	0.98	13.83±0.86	16.24±1.01
EL05-11	2.20±0.14	3.41	1.87	17.22	1	0.98	14.94±0.92	18.10±1.12
EL05-9	2.31±0.15	3.57	1.92	18.02	1	0.99	14.83±0.99	17.89±1.19
EL05-7	2.18±0.16	3.71	1.96	18.72	1	0.99	13.47±0.99	15.57±1.14
EL05-8	1.47±0.11	3.72	1.97	18.78	1	0.97	9.24±0.72	9.87±0.77
EL05-6	1.86±0.13	3.72	1.97	18.78	1	0.99	11.46±0.80	12.67±0.89

Appendix C

Laboratory Methods

Laboratory procedures for preparation of ^{10}Be target material

The procedure is modified from Licciardi (2000) and Rinterknecht (2003). A description of the phosphoric acid leaching step is now included, as well as procedures for major ion analysis via ICP-OES. The procedure describing oxidation of the samples has also been modified; however, the ion exchange procedure and necessary chemicals have not changed.

Throughout all of the steps below, safety and cleanliness are of the utmost importance. Contamination is a very real concern. Street shoes are not to be worn in the back part of room 115. Dedicated lab shoes should be left at the threshold for you to change into. Sweeping and dusting should be done regularly. Also avoid storage of cardboard in the lab. If you are not familiar with handling acids or any other part of the procedure **do not** proceed until receiving relevant training.

Isolation and cleaning of quartz from bulk rock

Before completing physical separation of quartz via crushing, pulverizing, sieving, and magnetic separation get instruction on safe use of the equipment.

Before crushing your samples, ensure you have measured the thickness of the sample, know its lithology, and taken any appropriate photos/notes. Crushing cannot be undone.

1) Crush rock in large **jaw crusher in room 038**. If the rock is too large to be put into the crusher, use hammer and chisel to reduce the size of the rock. Also, if the sample is very thick, use a rock saw to trim the lower portion off (be sure you are knowledgeable before using this machinery. Isolate the desired size fraction (the appropriate size depends on the lithology, but you should try to produce monomineralic grains) by dry sieving.

2) For the larger rock fragments that remain after crushing, use a **pulverizer** (disk mill) to produce mono-mineralic grains of as large a size as possible. Grains should be smaller than the average size of quartz grains (between 500 and 125 μm is suitable for most granitic rocks, quartz veins/ quartzite: 250-710 μm, typically finer grained rocks require finer size fractions). The fine fraction (< 250 μm) should be saved it in a labeled container. Removing it at this stage reduces the amount of acid consumed by dissolving it, and minimizes clogging of the magnetic separator. Continue pulverizing sample until all material has passed through the largest sieve. This step will need to likely be repeated multiple times. It is very important that the pulverizer spacing be slowly stepped down to avoid excess fines production. Doing so also maximizes sample size. Collect the fraction of interest in a clean plastic container.

3) Magnetic separation is performed in the mineral separation lab (room 021). Remove strongly magnetic minerals (magnetite, large amphiboles, etc.) with a powerful **hand magnet** and save in

a labeled container. Magnetite in particular is relatively unaffected during subsequent HF leaching and should be removed earlier.

4) Most rock samples, except quartzite and quartz veins, can have a significant proportion of mafic minerals. Remove these more weakly magnetic mineral phases using the **Frantz magnetic separator** and save in a labeled container. The Frantz is very adjustable; angles, feed speed, and magnetic strength can be adjusted. The most effective adjustments are 15-20° forward tilt, 10° side tilt, and magnet current at 0.5 amps. When operating the Frantz, remove all watches, and keep electronic devices a few feet away if you want them to work later. Do not operate without receiving instruction.

 For a typical granitic rock, these procedures separate out most of the amphibole and biotite, leaving behind a granular sample composed almost entirely of quartz and feldspar. These preliminary mechanical separations minimize the acid that is consumed by dissolution of the feldspar and mafic mineral phases in later steps.

5) Leaching of the sample in o-phosphoric acid is useful with samples that have high feldspar content because it dissolves some feldspar grains, but mostly serves to heavily etch the feldspar grains so that fewer HF leaching steps are needed. For quartzites, quartz sandstones, etc., this step is not necessary and you can proceed to HF/HNO_3 leaching. Complete this step in room 023. In 100 mL Pyrex beakers, weight out 50 g of sample into each beaker until enough material is weighed out to yield sufficient quartz quantities (4-6 beakers is usually needed). Add 400 mL of 85% o-Phosphoric acid to each beaker. Cover beaker with a watch glass and heat beakers on hotplates set to high. Bring to boil; boiling may be violent, so make sure to check on the beakers to prevent them from bouncing off the hotplate. During this initial boiling black foam may appear as water in the acid solution is boiling off. Boiling should subside after about 1 hour, as the o-phosphoric acid becomes pyrophosphoric acid.

 Boil for an additional 45 minutes, or until the volume reaches ~300 mL. Be careful at this point to not allow the acid to gelatinize (this will make rinsing incredibly difficult). If in doubt, stop boiling sooner rather than later. Remove beakers from hotplates and cool. A gel may have formed around the sample; this will be dissolved during the sodium hydroxide cleaning.

 Rinse watch glass with DI water and set aside. Add ~300 mL DI water to each beaker, stir with a clean micro-spatula to loosen gel around sample and on the side of the beaker. Drain the acid waste into the waste container using a funnel, being careful not to lose any sample. Repeat the above step. After this second rinse, rinse two more times with DI water and discard waste down sink. Almost all of the gel should be gone from around the sample.

 Add 200 mL 50% NaOH to each beaker, this will dissolve the gel that may have formed around the mineral grains during the Phosphoric acid leach. Boil sample on medium-high setting, once boiling, allow sample to boil for 10 more minutes. Boiling can be very violent, so it is necessary to watch the samples to prevent beakers from jumping off the hotplate. If boiling becomes violent, reduce hotplate temperature. Allow samples to cool for ~30 minutes. Drain NaOH solution into appropriate waste container. Rinse samples three times with DI water and discard waste down sink. Transfer samples from beakers into clean 250 mL beakers and dry overnight in the oven in room 021. Once the sample is dry, it is ready for HF/HNO_3 leaching.

6) In room 023 weigh 40 g of sample in a 4 L bottle. The number of bottles needed depends on the lithology of the sample; typically a minimum of 3 bottles with 40 g in each bottle should be used. It is preferable to use enough material so that the amount of clean quartz is sufficient for

two BeO targets (if necessary). For a quartz vein sample, 100 g of pulverized material is generally enough to provide clean quartz for two samples. For a quartzite rock use 100 to 150 g. For granitic rocks use 200 to 250 g. For rocks with very low quartz content such as rhyolites it may be necessary to use more than 250 g with 40 g in each bottle. Rinse well with MiliQ water to remove dust, fine fraction material and dry lichen. Fill the bottle with MiliQ water; add 40 mL conc. HF to make ~ **1% HF** and 40 mL conc. HNO_3 to make **~1%HNO$_3$. Always add acid to water, never the other way around!!!** Use an acid resistant lab coat, two pairs of vinyl gloves and an apron, safety goggles, acid fume mask, and other safety apparel when working with HF. Under **no circumstances** use HF unless you have received training in its proper use and how to handle acid burns and spills.

7) Under a fume hood, leave the sample bottles for ~24 hours in an ultrasonic tank with a water bath heated to ~60°C (or less). The ultrasonic tank must be run continuously during the leach. Leave screw tops slightly loose for ventilation. Be sure to use a hanging basket in the ultrasonic tank to prevent bottles from coming into contact with sides and bottom of the tank. Be sure to keep water level at its recommended level (no more than 1 inch below top lip) in the ultrasonic tank throughout the leach.

8) After each ~24h leach, carefully pour acid waste using large funnel into waste drum; **do not pour down sink!** Waste drums are available from Environmental Health Services; they will dispose of all acid waste (Call Environmental Health Services for more information). Avoid splashing. Be very careful that sample does not slump forward and out of bottle while decanting acid solution.

9) After decanting acid waste into waste drum, rinse the sample several times (2-3 times is sufficient, use more if the rinse water is heavy in "clay") with ultrapure water and discard fines with rinse water. Do this by filling the bottle with water, shaking vigorously, then allowing sample to settle before decanting the rinse water. Rinse the outsides of the bottles with tap water to remove any splashed HF/HNO_3. Remaining lumps should be crushed with a plastic spoon before proceeding to next leach. Some fines will unavoidably be lost with the rinse water.

10) Repeat steps 5 to 8. Usually, a total of 2 to 5 24-hour HF/HNO_3 leaches are necessary to obtain sufficient purity, depending on the sample lithology. There is no need to dry and weigh sample between each leach. Repeated leaching removes meteoric [10]Be, ensures sufficient purity for [26]Al measurement, and does not result in significant loss of quartz.

How to know when the sample is clean enough: When the sample looks clean and there is no lichen or suspended fine material ("clay") in the 1% HF/HNO_3 after leaching, remove a fraction of the sample with a spatula, dry it and inspect it under the microscope in room 021. The sample should be free of dark grains (magnetic minerals often have a metallic sheen). Quartz can be both translucent and opaque, and vary in color from white, gray, pink, yellow. Well-leached quartz grains often resemble partially melted ice, and the grains are less angular than the un-leached fraction. If grains of feldspar are still present they can be identified by a much more "eaten" and corroded surface.

11) After the last HF leach, rinse sample thoroughly and decant. Leave the bottles with clean quartz to dry in the laminar flow fume hood (room 115). Transfer the dried sample to a plastic

container. **Use only new or old acid-cleaned containers for storing the quartz separates. Avoid dust as much as possible.** To avoid loss of sample, it is best to use the wide-mouth plastic jars since the leaching bottle can simply be inverted into the jar. If only small jars are available, transfer quartz with a new plastic ice cream spoon.

12) If necessary, run dried quartz through the magnetic separator one last time to remove all remaining magnetic minerals. If this is done, place sample in a single 4 L bottle and leach in 1% HF/HNO_3 one last time (a 12-hour leach is sufficient). Dry in laminar flow hood and transfer to clean plastic container.

13) Rinse 4 L bottles and caps inside and out with distilled water (water and soap), remove labeling with acetone, and follow with a rinse of the inside with ultrapure water before storing.

ICP-OES Preparation Procedure

After leaching, each sample should be analyzed for major ion concentration. This is to ensure the sample is clean enough, and to measure the total Al concentration, which needs to be known if ^{26}Al is to be measured. To save money, it is best to run at least 20 samples through ICP-OES at one time.

In a clean 360 mL Teflon jar (this jar can be reused to dissolve the sample after sufficient purity is reached), weigh out ~0.1 g of the clean quartz and record the weight to 0.001 g in the notebook. Move jars to a fume hood and pipette ~5 mL of conc. HF into the jars (there must be enough HF in the jar to completely cover the quartz grains). Move jars with lids on to a hotplate and heat at a low setting until the quartz completely dissolves. Lids must not be vapor tight; completely tighten lids initially, then back off ¼ turn. Dissolution may take >4 hours. Depending on the sample lithology, some minerals may not dissolve completely; this is okay.

A blank should be prepared with the samples. Blank preparation follows sample preparation and the blank should be treated as if it were a sample.

Once the quartz has completely dissolved, remove lids, rinse with MiliQ water, dry with a Kimwipe, and store in Ziploc bag for later use. Evaporate samples to dryness. Evaporation can be accelerated with a heat lamp. Samples will have varying amounts of residue.

After the HF has completely evaporated, remove jars from hotplates and add ~2 mL of conc. HCl to each jar. Swirl jars to completely dissolve residue. Place jars back on hotplate and evaporate samples to near dryness. Repeat this step twice more. Repeated evaporations of HCl help to drive off any fluorides left from the dissolution. Allow jars to cool after the final evaporation.

Place a clean labeled 125 mL plastic bottle (pre-leach in 10% HNO_3 for at least 24 hours and rinse with MiliQ water) on the analytical balance and tare. Add 2 mL 10% HNO_3 to jar to dissolve residue, swirl to ensure complete dissolution. Repeat this step twice more to ensure complete removal of sample from Teflon jar.

Place bottle on analytical balance (do not re-zero balance); slowly and carefully add 10% HNO_3 to bottle until the mass is ~100 g (measure mass to 0.001 g). Note the final mass in the notebook.

Arrange time on the ICP-OES in COAS by contacting Andy Ungerer. If any of the ion concentrations, especially Al, is greater than 500 ppm, the sample should go through one more 24 or 48-hour leach. It is probably not necessary to analyze the sample again, unless [26]Al is to be measured, and then it is critical. Once sufficient quartz purity is achieved proceed to addition of Be carrier and sample dissolution.

Before samples can be analyzed on the ICP-OES, standards must be prepared and the machine calibrated. Elements to be measured are Be, Al, Fe, Ti, Ca, K, Na, and Mg. Standards can be reused multiple times; however, to ensure the concentration does not change due to evaporation, tightly cap bottles and wrap top of bottle with Parafilm.

Standards should be made by adding the volumes of 1000-ppm standard solution shown in the table below for each element. Record the mass of each element added, as well as the amount of **5% HNO_3** added to dilute the solution, ~100 mL should be added or up to ~100 g solution. Standard concentrations can then be calculated from mass of element added and amount of total solution, rather than by volume, to increase precision. Note that standard zero should be a blank with nothing added to the solution.

Target Standard Volumes

Element	Std 4 (µL)	Std 3 (µL)	Std 2 (µL)	Std 1 (µL)
Be	1000	500	50	5
Al	1000	500	50	10
Fe	1000	500	50	10
Ti	1000	500	50	10
Ca	100	60	10	5
K	10000	5000	500	100
Na	1000	500	50	10
Mg	500	100	10	5

Target Standard Concentrations

Element	Std 4 (ppm)	Std 3 (ppm)	Std 2 (ppm)	Std 1 (ppm)
Be	10000	5000	500	50
Al	10000	5000	500	100
Fe	10000	5000	500	100
Ti	10000	5000	500	100
Ca	1000	600	100	50
K	100000	50000	5000	1000
Na	10000	5000	500	100
Mg	5000	1000	100	50

Weighing Sample, Adding Be carrier and quartz dissolution in HF

Determine the appropriate weight of sample for analysis. A minimum of 10^6 ^{10}Be atoms is required for a good AMS measurement. The maximum amount of sample is limited by the volume of the Teflon jars. In general, use as big a sample as possible, between 40 and 60 g. This may be reduced in the future with the production of a low ^{10}Be carrier. Ideally half or less of the available clean quartz sample should be used, but this will not always be possible. In this study, 10-50 g of clean quartz were used depending on the clean quartz yield after leaching. Samples weighing 25-50 g of quartz were typical.

The amount of clean quartz needed will depend on the sample production rate, its estimated age, the ^{10}Be/^{9}Be background ratio in the AMS, and the ^{10}Be/^{9}Be ratio in the carrier, as well as the AMS lab making the measurements. More material is needed for young/low elevation samples than for old/high elevation samples.

Obtain a clean 360 mL Teflon screw top jar. Invert the ^{9}Be carrier (1000 μg/g) bottle a few times to homogenize the solution and to ensure that drops of condensation on the inside of the cap are mixed in. Place the Teflon jar on the balance without the lid, and re-zero (door will open). Set the Eppendorf pipettor to 250 μl and use a clean tip for each sample. Uncap the carrier bottle, and take care not to touch the inside if the bottle with the pipettor. Pipette 250 μl of the Be carrier solution into the Teflon beaker. Eject the carrier smoothly, being careful not to leave a drop in the tip. Close the door on the balance. Recap the carrier bottle as quickly as possible. **Record the weight (e.g. 0.250 g) on the sample log**. At the end of each session, screw the cap firmly on the Be carrier bottle and seal with Parafilm before storage.

Transfer the chosen amount of sample into the Teflon jar. **Record the weight (e.g. 40.000 g)** on the sample log. Sample should be well mixed before addition to ensure that the split taken is representative of the entire sample. Be careful of dust generated by pouring samples into the beaker as well as static charge on some of the quartz grains.

Add concentrated HF, 5 mL per gram of sample, to the Teflon jar containing the quartz sample. Be careful at this point not to splash or otherwise lose any solution. Tighten the lid down, then back it off ~$^1/_4$ turn. Place beaker on hotplate on low setting (~100°C) in fume hood. **The Teflon jar must not be gas-tight.** Do not swirl the contents of the jar at first; the initial reaction can be vigorous. **Never** shake the jar. Teflon should not be heated above 200°C, or you risk melting the bottle causing a large HF spill and the loss of the sample. Monitor hotplate temperature with a spot check surface thermometer.

Once the reaction has subsided (after a few hours), the hotplate can be turned up to ~150°C. From this point on, the jars can also be swirled occasionally to mix HF down into the dense H_2SiF_6 forming around the quartz grains. With the lids on, samples should dissolve completely in less than 24 hours, although some undissolved residue occasionally remains in some samples.

Preparation of blanks

Each batch of samples should include a blank. Prepare the blank as follows:

Obtain clean 360 mL Teflon screw top jar and add the same amount of Be carrier as was added to the samples. **Record the weight** to three decimal places, the mass of added Be carrier solution.

Add the same amount of acid as was added to the samples. For example, if the sample weight was 40g, and 200 mL HF was added to dissolve the sample, then 200 mL HF should be added to the Be carrier in the blank beaker. If a different amount of sample was used, add a midrange amount of acid to the blanks. From this point on, treat the blank in exactly the same manner as a regular sample.

Evaporation of HF and HClO₄

After dissolution, carefully remove the lid. There will be drops on the underside of the lid, and these should not be lost. The drops can be eliminated by tapping on the beaker top to knock them back into solution, and then by rinsing the insides of the lids with MiliQ water into the samples. Rinse lids (inside and out) in MiliQ water (do not add to sample), dry with Kimwipe and place in a clean plastic bag.

Evaporate samples to near dryness. Depending on the volume of solution this may take as long as 24 hours. **Do not leave beakers open overnight, or evaporate solutions overnight on the hotplate.** Once evaporated, a residue is usually left in the jar. For the blank sample this is usually just a tiny, white drop. For rock samples the amount of residue can vary from just a thin, white film or crust, to a white or slightly colored substance covering the bottom of the jar. Occasionally, the residue will be dark gray to black and have a metallic sheen. Proceed as instructed below, however it may be necessary to redissolve in HF.

Move Teflon jars to the hotplate **in a perchloric acid hood** (several jars may be placed on a single hotplate). Turn hotplate on medium-low (~150°C). Be sure nothing else is in the hood. With clean disposable pipettes, add **2 mL conc. HNO₃** and **1 ml of conc. TM HClO₄** to the solution in each Teflon jar and evaporate to dryness. The evaporation may take a whole day. The amount of residue is usually slightly reduced, but not significantly different at this stage compared to after the initial HF evaporation.

After the initial evaporation, add 2 mL conc. **TM HClO₄** to each Teflon jar, samples with a very large residue may require more). Swirl to dissolve, and return to the hotplate. Evaporate to dryness. Repeat this step once more, but with only 1 mL conc. **TM HClO₄**. The successive perchloric evaporations ensure removal of all fluorides from the sample.

Conversion to chloride form

Remove the Teflon jar from the hotplate. Using a disposable pipette, add ~ **2 mL of 6N HCl** (the exact amount is not critical, but should be consistent; samples with a very large residue may require a little more). The residue should re-dissolve instantaneously, and in most cases will go back into solution entirely after warming on the hotplate. If the residue does not re-dissolve it may be necessary to add ~ 10 mL conc. HF and check that the residue dissolves again, and then repeat the HClO₄ procedure. If nothing changes, you may have to do the conversion to chloride form and ignore the residue (see below).

Return the jar to the hotplate and evaporate to dryness. Repeat the **~ 2 mL 6N HCl** addition and evaporate a second time.

Re-dissolve a third time in **~ 2 mL 6N HCl**, then evaporate as close to dryness as possible. Avoid complete drying at the end of this step, in order to facilitate getting the sample back into solution for anion exchange. Do not be overly concerned, however, if drying is unavoidable.

Successive HCl evaporations should have eliminated fluoride (from the HF) and $HClO_4$ almost entirely. Fe, Ti, Al, Be, and other ions should be left as chloride salts ready for anion exchange. The final solution will generally be colored a deep yellow-green by $FeCl_3$. By the end of this procedure, however, some samples may have thrown a fine, powdery white TiO_2 precipitate that will not re-dissolve. No Al or Be is co-precipitated with the Ti, *which should be removed by centrifuging before anion exchange*. Often this precipitate can only be seen if the sample is transferred to a centrifuge tube (next step).

Transfer to centrifuge tube

Add **2 mL of concentrated TM grade HCl** to Teflon beaker, swirl to dissolve, and transfer carefully to clean labeled 15 mL centrifuge tube.

Add another **2 mL of concentrated TM grade HCl** and swirl to insure that sample residue in Teflon beaker has dissolved completely, and then transfer to centrifuge tube. Use as little liquid as possible (should be ~4 mL in the tube).

If you are not proceeding immediately to the column chemistry, keep tube covered with two layers of Parafilm and store in a clean cabinet.

Column setup procedure

Before embarking on the ion exchange procedures, the columns must be assembled. In order to successfully reproduce the column separations, it is imperative that the columns are filled with exactly the same volumes of resin as used in the development of the recommended procedures. In these procedures, separation is achieved by passing the dissolved sample through a resin-packed column (see attached materials list for the proper column supplies). Once set up, the resin can be used repeatedly for a large number of samples.

PACKING THE COLUMNS WITH RESIN:
Columns, stopcocks, and accessory funnels should be soaked overnight in cleaning solution (**10% HNO₃**) prior to setup. Clamp the column onto the stand, and screw the stopcock finger tight onto the column. Before introducing resin into the columns, it must be slurried with ultrapure water. To do this, add a small amount of resin to a clean plastic container, and add enough ultrapure water to form a loose slurry. Fill the column part-way with water, open the stopcock valve, and pour the slurried resin into the column in small additions. The resin should settle out gradually and evenly as it is added; do not to allow the resin to settle out completely between additions, as

this may result in heterogeneities in the resin packing. Continue to add slurried resin to the column until the proper volume is reached. If too much resin is added, adjust resin volume with a disposable pipette.

ANION COLUMNS:

Fill the anion columns with anion exchange resin until the level is ~1 mm below the upper plastic bushing of the Econo-Column (for type of column, see supplies list at end); this is equivalent to approximately 7 mL resin. All anion columns must have exactly the same volume of resin in order to achieve consistent results. The resin volume will shrink and swell as different acid concentrations are added, and should eventually equilibrate to a level ~4-5 mm below the upper plastic bushing of the column. It is imperative that new resin is thoroughly rinsed with concentrated TM grade HCl in order to flush out organic material that bleeds from the resin in strong acid. The organic material will be clearly visible as orange-brown residue in the eluate. To precondition new anion resin, first run **30 mL 1N HCl** through the column as a preliminary cleaning measure, and then add **concentrated TM grade HCl** in portions of 50 mL until the eluate runs clear (should require less than 200 mL). Following this, perform one entire anion procedure (described below), but with no sample. Only after this preconditioning should the column be used for an actual sample.

CATION COLUMNS:

Fill the cation columns with exactly 10 mL cation exchange resin; the level should be ~118 mm above the lower plastic bushing of the Econo-Column (for type of column, see list at and). After filling the first column, use a permanent marker to mark an equivalent level on all cation columns to be filled, so that each has exactly the same volume of resin. As with anion resin, it is imperative that new cation resin is preconditioned in order to flush out organic material, although the material that bleeds from the cation resin is not as clearly visible as that from the anion resin. In order to precondition new cation resin, first run **30 mL 0.6N HCl** through the column as a preliminary cleaning measure, and then add portions of 50 mL **6N HCl** until the eluate runs clear (should require less than 200 mL). Once the 6N HCl has drained through, add **50 mL of 1N HCl** to the column to allow gradual expansion of the resin. Following this, perform one entire cation procedure (described below), but with no sample. Only after this preconditioning should the column be used for an actual sample.

WHEN TO CHANGE THE RESIN:

After preconditioning, the resin can be used indefinitely for ion exchange, as long as it is properly cleaned between samples. There are, however, two common circumstances when the resin should be changed.

1) The cation resin volume shrinks and swells more dramatically than anion resin as different buffer strengths are added, which creates potential problems in maintaining homogeneity of resin packing. The procedures are designed to minimize these shrink-swell problems, however sometimes the level of the cation resin does not rebound to its former volume (which should be marked with a permanent marker) at the end of a cation procedure, and the flow rate becomes

restricted. If the column is filled with ultrapure water and allowed to soak overnight, the resin volume will usually rebound. If it does not, the resin must be discarded and replaced. Occasionally this problem can be solved by removing the resin and repacking the column with the same resin, and this should be tried first.

2) A discoloring of resin that persists after thorough column cleaning indicates that undesirable ions are permanently trapped in the column. This is most common in the anion columns. The discolored resin should be discarded and replaced. It is sometimes sufficient to draw out just the upper portion of the resin bed with a disposable pipette, and then refill the column with new resin up to the former volume.

Repacking of columns can take a very long time and slow sample processing greatly. In order to avoid slowdowns, keep at least three columns packed and ready to be used as backup columns.

STORAGE OF RESIN PACKED COLUMNS:
If you know that you are not going to use the ion exchange columns for some time (weeks), they should be stored properly to avoid drying or dust contamination. **Drying is bad and will requiring repacking the columns!!** Remove the funnels (which can be cleaned and stored in clean plastic bags); fill the columns with ultrapure water, cover with yellow caps and seal well with Parafilm.

AFTER STORAGE:
If the columns have not been used for many weeks or months: If the resin is dry it must be changed. If the columns still have water above the level of the resin; check that they are working well before you start with your samples. Do this by performing an entire anion and cation procedure, without sample. If the residue contracts and expands as expected, and the drip rates are uniform for all columns, then proceed as usual.

Before beginning the anion and cation column procedures, make enough reagents to run all samples through the columns. An appropriate amount for 6 anion and 6 cation columns is ~5 L of 1N HCl, ~5 L of 0.6N HCl, and 2 L of 6N HCl. This volume of reagent should be enough to run 12 samples through the columns.

<u>**Anion exchange column procedure**</u>

COLUMN PREPARATION:
Run **30 mL 1N HCl** through the column as a preliminary cleaning measure. Discard the eluate in the HCl waste bottle.

Condition the column with **30 mL concentrated TM grade HCl**. Once the solution has drained through, discard the eluate in the HCl waste bottle.

Rinse a clean 250 mL Teflon beaker with ultrapure water (if beaker has been stored in 10 % HNO_3 bath) and label (use tape) the sample name. Beakers should be cleaned previously after you

are finished using them. Rinse a new 125 mL plastic bottle with 10 % HNO_3 and then with ultrapure water, and label with the sample name and the date. Label this bottle "Anion Eluate."

LOADING THE SAMPLE:
Centrifuge the tube containing the chloride-converted sample for 10-15 minutes at high speed in the Fisherbrand or Medilite centrifuge. This will remove all insoluble residues from the sample solution.

Place the Teflon beaker under the column and make sure the valve is open. **Carefully and slowly pour sample directly from centrifuge tube into column, leaving behind insoluble residue at the bottom of the tube**. Allow solution to draw into the resin. Do not reuse the centrifuge tube.

Add **10 mL concentrated TM grade HCl** to the column and collect eluate in the beaker. Add another **10 mL concentrated TM grade HCl** to the column and collect eluate in the beaker.

Place the beaker on a hotplate at low heat (~120°C), and evaporate to dryness. Some samples may take on a brownish orange hue that indicates the presence of oxidized organic material. Dry down each sample three times with **~ 2 mL 6N HCl**. The samples are now ready for cation exchange.

CLEANING THE COLUMN:
Place the "Anion Eluate" bottle under the column and add **60 mL 1N HCl** (in two 30-mL additions) to the column. The resin should return to its original color and the eluate should appear clear after the second 30 mL has gone through the resin (the first half of the first 30 mL is often yellow). If it does not, continue adding more 1N HCl. Save eluate in the plastic bottle.

Add **50 mL ultrapure water** to the column. Discard eluate. Add a few mL of ultrapure water to the column to keep the water level above the level of the resin and cover (lid/ Parafilm) to prevent the resin from drying out.

Cation exchange column procedure

COLUMN PREPARATION:
Run **50 mL ultrapure water** through the column as a preliminary cleaning measure.

Add **30 mL 0.6N HCl,** this is to condition the column before adding the sample. The eluate is discarded in the HCl acid waste bottle.

Rinse two new 125 mL bottles, using 10 % HNO_3 followed by ultrapure water, and label with the sample name and date. Label one 125 mL bottle "Cation Eluate" and label the other 125 mL bottle "Al Fraction."

SAMPLE PREPARATION:
Add **2 mL 0.6N HCl** to the Teflon beaker containing the final product of the anion exchange procedure and swirl to ensure that the entire residue inside the beaker has dissolved. Transfer

contents to a centrifuge tube by carefully pouring; the liquid should form a single bead and roll smoothly out of the Teflon beaker.

Add another **1 mL 0.6N HCl** to the Teflon beaker, swirl, and transfer the rinse to the centrifuge tube (should be ~3 mL in the tube). At this point some samples may be clouded with a fine white precipitate, which must be removed before introduction into the cation columns, often the precipitate is not easily seen until after centrifuging. Centrifuge for 10-15 minutes.

LOADING THE SAMPLE:
Place the "Cation Eluate" bottle under the column and make sure the valve is open. Use a disposable pipette to transfer the sample from the centrifuge tube to the resin bed, being careful not to draw any white precipitate into the pipette. Add the solution to the resin 1 mL at a time and allow it to draw into the resin between additions.

COLLECTING THE FRACTIONS:
Add **130 mL of 0.6N HCl** to the column reservoir and allow to drain through, being careful to minimize disturbance of the upper surface of the resin bed. Collect in the "Cation Eluate" bottle (125 mL bottle is ok).

Place a clean Teflon beaker (clean, rinse and dry the beaker previously used) for the Be fraction under the column, and add **100 mL of 0.6N HCl** to the column reservoir. Once the elution is complete, place the beaker on a hotplate at about 120°C, and evaporate to dryness. The evaporation process will take >5 hours, although can be accelerated with a heat lamp.

Add **50 mL of 6N HCl** to the column reservoir and collect in the "Al Fraction" bottle.

Add **50 mL of 6N HCl** to the column reservoir and collect in the waste bottle. Save the bottles with the Al fraction and Cation eluate for future processing and/or ICP analysis.

CLEANING THE COLUMN:
Add **50 mL of 1N HCl** to the column. Discard eluate. The addition of weak acid before adding water will allow a gradual expansion of the resin and prevents rapid and uneven constriction of pore spaces.

Add **100 mL of ultrapure water** to the column. Discard eluate. Add a few mL of ultrapure water to the column and cover to prevent the resin from drying out.

After cleaning the columns, the resin may not completely rebound to their original height. Allow water to remain in the resin overnight; this should resolve the issue. If it does not, repack the column with the current resin. If the problem still persists, repack the column with new resin.

Precipitation of Beryllium Hydroxide

Always wear gloves when handling the sample, and keep the centrifuge tube and crucible covered as much as possible to avoid contamination by dust.

TRANSFER TO CENTRIFUGE TUBE:

Add **2 mL of 0.6N HCl** to the Teflon beaker containing the final product of the cation exchange procedure and swirl to ensure that the entire residue inside the beaker has dissolved. Transfer contents to a centrifuge tube by carefully pouring; the liquid should form a single bead and roll smoothly out of the Teflon beaker. Add **1 mL of 0.6N HCl** to the beaker, swirl, and transfer rinse to centrifuge tube, repeat by adding **1 mL of 0.6N HCl** once more. Bring solution volume up to 5 mL by adding **1 mL MiliQ water** to the centrifuge tube and mix well on the vortex mixer.

REMOVAL OF Ti:

Add concentrated TM grade NH_4OH to solution, mixing it on the vortex mixer, until the solution reaches pH ~5 (this should require **~200 to 300 μL NH_4OH**). To check the pH, remove 5 μL of the sample with a pipette (being careful not to touch the inside of the centrifuge tube with the pipette shaft) and apply to pH indicator paper. If the pH shoots past 5, adjust acidity by adding drops of **1:1 HNO_3:H_2O** and re-check the pH. If the sample contains Ti, a white precipitate will form. Centrifuge for 15 minutes. Pour supernatant into another clean centrifuge tube labeled "Be" and save. Re-label the old tube with the precipitate as "Ti" and set aside.

PRECIPITATION OF Be(OH)$_2$:

Add NH_4OH to supernatant in the Be tube, mixing it on a vortex mixer, until the solution reaches pH ~8 and a white $Be(OH)_2$ precipitate has formed (this should require **~50 μL NH_4OH**). Mix well on the vortex mixer. The precipitate can be hard to see. The liquid will be clouded, however, it is often easier to identify the precipitate by looking at the walls of the centrifuge tube above the liquid.

Centrifuge for 15 minutes. Pour supernatant into the centrifuge tube labeled "Ti" and save. Be careful not to pour out any precipitate. Use a 30 mL plastic bottle for collecting and storage of all supernatant fractions from one sample. All supernatants are collected in the event that there is poor Be yield in the final precipitation. If poor yield is encountered, the supernatant can be reprecipitated and additional Be may be recovered by repeating the beryllium hydroxide precipitation steps.

Add **100 μL of 1:1 HNO_3:H_2O**, swirl on a vortex mixer until precipitate has dissolved completely, and then bring solution volume up to ~5 mL by adding ultrapure water to the centrifuge tube. Swirl again on a vortex mixer.

Re-precipitate $Be(OH)_2$ by adding **~200 μL NH_4OH**. Mix well on the vortex mixer.

Centrifuge for 15 minutes. Pour supernatant into the "Ti" centrifuge tube.

All procedures from this point forward should be completed in the clean hood

Bring solution volume up to **5 mL** by adding **pH 8 water** to the centrifuge tube, swirl on vortex mixer to slurry, centrifuge for 15 minutes, and pour supernatant into the "Ti" centrifuge tube or a bottle. Repeat this rinsing step twice more. Repeated washing and rinsing of the precipitate should help remove possible boron contamination from the sample. (Make pH 8 water by adding NH_4OH to MiliQ water). Before using pH 8 water after it has been sitting for an extended time, check the pH to ensure it is still at pH 8.

After the final rinse, try to remove as much liquid from the centrifuge tube as possible. If you are not proceeding immediately to the oxidation step, keep tube covered two layers of Parafilm and store in the laminar flow clean hood.

Oxidation of Beryllium Hydroxide for analysis at Gif sur-Yvette
Note that this step is designed to work for samples prepared for analysis at the CNRS Tandetron Facility. If you will be measuring Be concentrations elsewhere, check with that lab and adjust procedures as necessary. Procedures for the CAMS facility at Lawrence Livermore National Lab are documented elsewhere and available from Ed Brook.

Quartz crucibles and caps should be cleaned in **10% HNO$_3$** and rinsed in ultrapure water before use, then dried on a hotplate in the clean hood at a medium-low temperature for 30 minutes. This will remove any boron that may be on the outside surface of the quartz. The caps may be used again, but they should be cleaned in 10% HNO$_3$ for at least an hour between uses. The crucibles will not be reused for other samples.

TRANSFER TO CRUCIBLE:
Obtain a new quartz crucible and weigh it on an analytical balance to 0.0001 g. Allow crucibles to cool to room temperature before weighing. **Record the weight** in notebook.

Add **200 μL 10% HNO$_3$** to the final precipitate in the centrifuge tube. This will dissolve the precipitate. Mix on a vortex mixer to form slurry, and carefully pour the slurry into the quartz crucible. Rinse the centrifuge tube again with **200 μL 10% HNO$_3$**, swirl, and pour the rinse into the crucible. Repeat the previous step one last time. Evaporate to dryness at a low (<100°C) setting. Initial evaporation at low temperature avoids boiling and splattering of the sample. **The sample is very vulnerable to contamination at this stage, and the evaporation should be conducted in a clean air hood if possible.** The sample material may become white and powdery.

After the initial evaporation turn the hotplate at maximum setting (~ 400-450°C) for about 30 minutes. After this, let the hotplate cool down to room temperature before you remove the crucibles. Cover the crucibles with quartz caps. If you are not proceeding immediately to the oxidation, seal the crucible and cap with Parafilm.

Place the crucibles inside the rapid mineralizer set at 999°C, and heat for 1 hour to convert all of the material to BeO. Cover the crucibles with quartz caps during the heating to avoid contamination by dust. The labels will burn off, so be sure to write down the arrangement of the labeled crucibles inside the mineralizer. If necessary the samples can be sorted out based on the initial crucible weights, but do not rely on this.

Wait until the crucible is completely cool (room temperature), remove cap, then re-weigh the crucible containing the sample to four decimal places. **Record the weight** in notebook. After weighing, cover with several layers of Parafilm. Label the crucible, and then place the sample in a clean container. Calculate % yield by comparing the expected weight from the amount of Be carrier added with the recorded weight after oxidation.

For example, using 0.25 g of 1000 μg/g Be carrier solution provides:

$$0.25g \times \frac{1000 \mu g}{g} Be \times \frac{1g}{1 \times 10^6 \mu g} = 0.25 \times 10^{-3} gBe.$$

When converted to expected yield of BeO it is:

$$0.25 \times 10^{-3} gBe \times \frac{1 \text{ mol Be}}{9.01218 \text{ g}} \times \frac{25.01158 \text{ g BeO}}{\text{mol}} \approx 6.94 \times 10^{-4} \text{ g BeO}$$

$$\% \text{ yield} = \frac{\text{measured yield}}{\text{expected yield}} \times 100$$

Cleaning of Teflon jars and beakers: Clean inside and outside with distilled water and lab soap. Rinse in ultrapure water. Dry with Kimwipe. Fill Teflon jars with **10% HNO$_3$**. Leave the Teflon for minimum 24 hours. Pour the used 10% HNO$_3$ in the HNO$_3$ acid waste container. Rinse all Teflon three times in ultrapure water. Store in plastic bags if not used immediately.

Cleaning of other items: The 4L plastic bottles used for leaching should be rinsed multiple times with DI water to ensure all quartz is removed. Lids should also be rinsed with DI water. Dry and store on plastic shelves in room 023. Eluate bottles should be kept until ^{10}Be has been measured. Afterwards, eluate can be disposed of is acid waste drum, bottles rinsed with water and recycled. Any other labware should be cleaned with lab soap, rinsed in DI water and dried.

Chemical Reference Sheet

Note: the recipes for 0.6, 1, and 6 N HCl follow the simplifying approximation that concentrated HCl has a normality of 12 (the actual value is ~12.1). The logic behind this simplification is that it allows measurement of "round-numbered" volumes for the working solution recipes (e.g., 100 mL instead of 96.2 mL), which presumably will decrease the chance for inaccurate or mistaken measurements. All procedures described above, as well as the column calibrations, were performed using the recipes given below; hence these must not be modified without recalibrating the columns.

Parent Reagents:

Name	Formula	Usual % strength of concentrated reagent	Normality	Grade
Hydrochloric Acid	HCl	35-38% w/w	12.1 N	TM
Nitric Acid	HNO_3	68-71% w/w	15.9 N	TM
Hydrofluoric Acid	HF	49% w/w	28.9 N	ACS
Hydrogen Peroxide	H_2O_2	31% w/w	9.8 N	ACS
Perchloric Acid	$HClO_4$	69-72% w/w	11.7 N	TM
Ammonium Hydroxide	NH_4OH	20-22% w/w	14.5 N	TM

Working Solutions:

Label	Uses	Recipe
"10% HNO_3"	**ICP analysis stock solution; general purpose cleaning solution.**	**1800 mL water + 200 mL conc. TM grade HNO_3**
"0.6 N HCl"	**Cation columns - conditioning, loading and Be elution.**	**1900 mL water + 100 mL conc. TM grade HCl (950 mL water + 50 ml conc. HCl)**
"1 N HCl"	**Anion columns - pre-cleaning and stripping. Cation columns - post-cleaning and conditioning.**	**1100 mL water + 100 mL conc. TM grade HCl (916.7 mL water + 83.3 mL conc. HCl)**
"6 N HCl"	**Cation columns - Al elution and stripping. Conversion of samples to chloride form.**	**Equal parts water + conc. TM grade HCl (500 mL water + 500 ml conc. HCl)**
"TM grade HCl"	**Anion columns - conditioning, loading and Be elution.**	**Conc. TM grade HCl**
"TM grade NH_4OH"	**Beryllium hydroxide precipitation.**	**Conc. TM grade NH_4OH**
"1:1 HNO_3"	**Beryllium hydroxide precipitation.**	**Equal parts water + conc. TM grade HNO_3**
"1:1 $HClO_4$"	**Dry-down oxidations.**	**Equal parts water + conc. $HClO_4$**

Basic Facilities and Equipment at OSU
Braun Chipmunk (jaw crusher), room 038
Bico Pulverizer Type UA (disk mill), room 038
USA Standard Testing Sieve Set, room 019
Frantz Isodynamic Separator, model L-1, room 021
Large hand magnet, room 021
Milli-Q water dispenser, room 115

Standard (room 021, 023), perchloric acid (room 115), and laminar flow hoods (room 115)
Four Aquasonic ultrasound tanks, model 7500
Mettler Toledo AT460 (Delta Range), analytical balance
Cimarec 3 hot plates, Thermolyne
Spot check surface thermometers
Vortex mixer
Fisher Centrific Model 228 bench top centrifuge
Eppendorf Series 2100 Pipettors, 5, 50, 200, 1000 µL
Rapid incinerator/mineralizer/oxidizer, model Schellervashcer

Ion-Exchange Column Supplies (see column setup procedure)
Econo-Column chromatography columns:
    1.0 cm inner diameter, 10 cm length, Bio-Rad Cat.# 737-1011 (anion columns)
    1.0 cm inner diameter, 20 cm length, Bio-Rad Cat.# 737-1021 (cation columns)
Bio-Rad resins:
    AG 1-X8 Resin, 100-200 mesh, chloride form, Bio-Rad Cat. #140-1441 (anion exchange resin)
    AG 50W-X8 Resin, 100-200 mesh, hydrogen form, Bio-Rad Cat.# 142-1441 (cation exchange resin)
Econo-Column funnels, Bio-Rad Cat.# 731-0003 (one per cation column)
Bio-Rad 2-Way stopcocks, Bio-Rad Cat.# 732-8102 (one per column)

Miscellaneous Laboratory Materials
Savillex 360 mL Teflon jars, Savillex part # 0112 (for quartz dissolution)
Teflon PTFE beakers, 250 mL (for eluate collection)
Nalgene 4 L polypropylene bottles (for preliminary acid leaching)
Nalgene HDPE 125 mL bottles (for collection and storage of eluate)
Nalgene 25 L LDPE carboy with spigot (for storage of ultrapure water)
Nalgene polypropylene graduated cylinders: 1000, 500, 250, 100, 50, 10 mL
Plastic containers (for storage of purified quartz)
Disposable transfer pipettes, 5 mL
Nalgene centrifuge tubes15 mL (for centrifuging)
pH indicator paper, Whatman Type CF strips
Quartz crucibles, 10 mL from California Custom Glass
Quartz crucible caps, from California Custom Glass
Nalgene wash bottle, 500 mL (for accurate volume delivery of ultrapure water)
Parafilm
Neoprene apron
Heavyweight disposable vinyl gloves
Safety goggles or face shield

Appendix D

All ages contained in this thesis were calculated using the MATLAB program "agecalc10.m". This code can be used to calculate [10]Be exposure ages for samples run on Tandetron Accelerator Facility at Gif sur-Yvette.

AGECALC10: Calculates age and calls other functions

```
%AGECALC10
%  AGECALC10 calculates exposure ages for the nuclide 10Be.  Other inputs are
%  nuclide
%  production rates (calculated from function 'scaling'), and the nuclide
%  concentrations in atoms/g quartz. Output is inputted data, 10Be concentration,
%  Production rate, scaling factors, 10Be age, and uncertainty.

%Copyright Brent M Goehring
%Oregon State University, 2005


%Constants
att = 155; %g/cm2
l10 = 4.62098e-7; %yr-1

%Creates a text file to output the sample data.
file = input('Enter the file output name.','s');
fid = fopen([file '.txt'],'a');
line1 = 'Sample Name,Lat (degrees),Alt (m),Sample Wt (g),Spike Wt (g),Be
Ratio,#Counts,10Be Atoms (at),Atoms Unc (at),Conc (at/g),Conc Error
(at/g),Neutron,Muon,Prod (at/g/yr),Shield,Thick,Age (yr),Plus (yr),Minus (yr)\n';
fprintf(fid,line1);

%Prompts user for number of samples to be calculated
n_samples = input('How many samples do you wish to calculate? ');
blank = input('What is the average number of 10Be atoms in the blanks?\n (This is
subtracted from total #of atoms in a sample.) ');
blank_unc = input('What is the uncertainty of the blank average (atoms)? ');


for i = 1:n_samples
    %The section below will prompt the user for the appropriate information to
    %calculate a 10Be age.
    sampleName = input('What is the sample name? ','s');
    sampleWt = input('What is the mass of quartz dissolved? ');
    spike = input('What is the mass of the spike? ');
```

```
ratio = input('What is the measured 10Be/9Be ratio? ');
events = input('How many 10Be events were counted? ');
alt = input('What is the elevation of the sample (m)? ');
lat = input('What is the latitude of the sample (degrees)? ');
rho = input('What is the approximate density of the sample (g/cm2)? ');
z = input('What is the thickness of the sample (cm)? ');
geom = input('Enter the horizon geometry as a 2 by n matrix.\n Sector widths should
appear in the first row, and corresponding inclinations in the second row. ');
    %Prompts user and asks if they wish to input an erosion rate to
    %calculate an age.
    if input('Do you wish to calculate an age with erosion rate? [y/n] ','s') == 'y'
        E = input('What is the erosion rate (g/cm^2 yr)? ');
    else
        E = 0;
    end

    %The section below will call the necessary functions to get production rate
    %Calculates the local production rate based on the alt/lat scaling,
    %shielding, and thickness corrections.
    [p10_local, spall_fac, muon_fac] = scaling(alt, lat);

    %Calculates the shielding correction
    hor = horiz(geom);

    %Calculates the thickness  correction
    thick = expSurf(z, rho);

    %Net production rate the product of the scaled production rate, shielding
    %correction, and thickness correction.
    p10_site = p10_local * hor * thick * (26.8/30.6);

    %Calculate the number of atoms
    total_atoms = ams(sampleWt, spike, ratio, blank);

    %Calculates the relative uncertainty based on the number of 10Be events
    mach_unc = (1 / sqrt(events));

    %Calculate total uncertainty with machine error and blank uncertainty
    %propogated. No blank uncertainty yet.
    unc = sqrt(mach_unc^2 + 0.05^2);

    %Concentration uncertainty is calculated in atoms
    atoms_unc = total_atoms * unc;
```

```
%Propogate the blank uncertainty into the measurement now (atoms)
total_unc = sqrt(atoms_unc^2 + blank_unc^2);

%Calculate total relative uncertainty (percent)
relative_unc = total_unc / total_atoms;

%Convert everthing to atoms per gram now.
conc = total_atoms/sampleWt;

%Concentration uncertainty
conc_unc = conc * relative_unc;

%Calculate the simple continuous minimum exposure age.
sample_age = -(1/(l10+(E/att)))*log(1-(l10+(E/att))*(conc/p10_site));

%Instead of simply assuming the age is in the linear portion of the curve,
%this program calculates the +/- error asymetrically, thus some errors around
%a sample will not be symetric if the sample is old.
conc_up = conc_unc+conc;
conc_down = conc-conc_unc;

plus_error = -(1/(l10+(E/att)))*log(1-(l10+(E/att))*(conc_up/p10_site)) - sample_age;
minus_error = sample_age - (-(1/(l10+(E/att)))*log(1-
(l10+(E/att))*(conc_down/p10_site)));

%Formats the data to be printed to a file.
altout = sprintf('%1.0f\t',alt);
latout = sprintf('%1.0f\t', lat);
pout = sprintf('%3.2f\t',p10_local);
neuout = sprintf('%1.2f\t',spall_fac);
muout = sprintf('%1.2f\t',muon_fac);
eventsout = sprintf('%1.0f\t',events);
wtout = sprintf('%1.3f\t',sampleWt);
spikeout = sprintf('%1.3f\t',spike);
ratioout = sprintf('%1.3e\t',ratio);
atomsout = sprintf('%1.3e\t', total_atoms);
atomsuncout = sprintf('%1.3e\t', total_unc);
horout = sprintf('%1.2f\t',hor);
thickout = sprintf('%1.2f\t', thick);
concout = sprintf('%1.3e\t',conc);
uncout = sprintf('%1.3e\t', conc_unc);
ageout = sprintf('%1.3e\t', sample_age);
plusout = sprintf('%1.3e\t', plus_error);
minusout = sprintf('%1.3e\t', minus_error);
```

```
    %conc_uncout = sprintf('%1.2`f\t', relative_unc);
    fprintf(fid, '%s\t', sampleName);
    fprintf(fid,'%s\n',[latout, altout, wtout, spikeout, ratioout, eventsout, atomsout,
atomsuncout, concout, uncout, neuout, muout, pout, horout, thickout, ageout, plusout,
minusout]);
end

fclose(fid);
```

AMS: Reduces accelerator data

```
function [conc, unc, conc_up, conc_down] = ams(sampleWt, spike, ratio, blank)

%AMS
%AMS is a function that calculates the 10Be concentration of a sample as
%well as the uncertainty of the measurement based on counting statistics
%and propogation of counting stats and 5% machine uncertainty. Inputs are
%the mass of quartz used, the mass of the 9Be spike, the 9Be/10Be ratio,
%and the number of 10Be events counted.

%This section calculates the concentration of 10Be in the sample.
N9Be = spike * 1000; %ug 9Be
N9Be = N9Be * (1/(1*10^6)) * (1/9) * 6.022e23; %Number of 9Be atoms
conc = ratio * N9Be;
conc = conc - blank;


function [p10_local, spall_fac, muon_fac] = scaling(alt, lat)
```

SCALING: Calculates scaling factors for sampling location

```
%SCALING -
%   SCALING(alt, lat) calculates total production rate for Be-10 and Al-26
%   via spallation and muons. Inputs are simple and consist of sample
%   altitude (m above sea level = 'alt') and latitude (degrees = 'lat').
%   Total production rate is found using the Lal (1991) polynomials
%   modified by Stone (2000) for atmospheric presssure differences.
%
%   Example: [p10_local, p26_local] = scaling(0, 60)
%       p10_local = 5.1
%       p26_local = 31.1
%
%   Brent M. Goehring
%   2005
```

```
%Constants
p10Be = 5.1;  %atoms/g/yr at sea level high latitude
p26Al = 31.1; %atoms/g/yr at sea level high latitude
Ps = 1013.25; %sea level pressure (hPa)
Ts = 288.15; %sea level temperature (K)
lr = 0.0065; %adiabatic lapse rate (K/m)
K = 0.03417; %gM/R (K/m)

%Calculates the local atmospheric pressure
P = Ps*exp(-(K/lr)*(log(Ts)-log(Ts-lr*alt)));

%polynomial scaling of production via production with latitude and altitude
lalpoly = [31.8518, 250.3193, -0.083393, 7.4260e-5, -2.2397e-8;...
    34.3699, 258.4759, -0.089807, 7.9457e-5, -2.3697e-8;...
    40.3153, 308.9894, -0.106248, 9.4508e-5, -2.8234e-8;...
    42.0983, 512.6857, -0.120551, 1.1752e-4, -3.8809e-8;...
    56.7733, 649.1343, -0.160859, 1.5463e-4, -5.0330e-8;...
    69.0720, 832.4566, -0.199525, 1.9391e-4, -6.3653e-8;...
    71.8733, 863.1927, -0.207069, 2.0127e-4, -6.6043e-8];


poly_a = [];
poly_b = [];

%Series of if statements that selects the correct lower and upper
%polynomial coefficents.
if lat < 10
        poly_a = 1;
        poly_b = 2;
elseif lat < 20
            poly_a = 2;
            poly_b = 3;
elseif lat < 30
            poly_a = 3;
            poly_b = 4;
elseif lat < 40
            poly_a = 4;
            poly_b = 5;
elseif lat < 50
            poly_a = 5;
            poly_b = 6;
elseif lat < 60
            poly_a = 6;
            poly_b = 7;
```

```
else
        poly_a = 7;
        poly_b = 7;
end

%Inserts correct coefficients into fourht order polynomials for upper and
%lower latitude limits.
poly1 = lalpoly(poly_a,1)+(lalpoly(poly_a,2)*exp(-
P/150))+(lalpoly(poly_a,3)*P)+(lalpoly(poly_a,4)*P.^2)+(lalpoly(poly_a,5)*P.^3);
poly2 = lalpoly(poly_b,1)+lalpoly(poly_b,2)*exp(-
P/150)+lalpoly(poly_b,3)*P+lalpoly(poly_b,4)*P^2+lalpoly(poly_b,5)*P^3;
%Interpolates between 10 degree latitude bands so intermediate latitudes
%can be used.
scale_wt = ceil(lat/10) - (lat/10);
spall_fac = scale_wt * poly1 + (1 - scale_wt) * poly2;


%Now scaling for muons

%Muon production latitude factor
lat_fac=[.587;.600;.678;.833;.933;1.000;1.000];

poly_c = [];
poly_d = [];

if lat < 10
    poly_c = 1;
    poly_d = 2;
elseif lat < 20
    poly_c = 2;
    poly_d = 3;
elseif lat < 30
    poly_c = 3;
    poly_d = 4;
elseif lat < 40
    poly_c = 4;
    poly_d = 5;
elseif lat < 50
    poly_c = 5;
    poly_d = 6;
elseif lat < 60
    poly_c = 6;
    poly_d = 7;
else
```

```
    poly_c = 7;
    poly_d = 7;
end


poly3 = lat_fac(poly_c)*exp((Ps-P)/242);
poly4 = lat_fac(poly_d)*exp((Ps-P)/242);
muon_fac = scale_wt * poly3 + (1-scale_wt) * poly4;



%Calculates the total isotope production based on the fraction spallation
%and fraction muogenic production
fspall_be = 0.974;
fspall_al = 0.978;

%Calculate the scaling factor and production for Be
F_be = fspall_be*spall_fac+(1-fspall_be)*muon_fac;
p10_local = p10Be*F_be;

%Calculate the scaling factor and production for Be
F_al = fspall_al*spall_fac+(1-fspall_al)*muon_fac;
p26_local = p26Al*F_al;

function hor = horiz(geom)
```

HORIZ: Calculates correction for shielding by topography

```
%HORIZ
%   HORIZ(geom) calculates the shielding due to topography. Input geom is a
%   n by 2 matrix consisting of the width between azimuthal directions in
%   row one and the inclination in degrees of each azimuth in row 2. The
%   sum of row one must equal 360 and inclination values cannot exceed 90
%   degrees. Equations for topographic shielding follow those in Nishiizumi
%   et al., 1989.
%
%   Brent M Goehring
%   2005

%Check to make sure that there is data for 360 degree field of view.
if sum(geom(1,:)) ~= 360
        disp('WARNING! Azimuthal horizon data do not add up to 360 degrees!')
end

%Check to make sure that the inclination is not greater than 90 degrees or
%less than 0 degrees.
```

```
for b = 1:size(geom,2)
        if geom(2,b) > 90 | geom(2,b) < 0
                disp('WARNING! Elevational horizon data are not in the range of 0 - 90
degrees!')
        end
end

%Set initial correction to zero.
hor = 0;

%Converts inclination and azimuths to radians.
geom = geom .* (2*pi/360);

%Calculates the amount blocked by topography.
for a = 1:size(geom,2)
        hor = hor + geom(1,a)/(2*pi) * (sin(geom(2,a))^3.3);
end

%Results in the fraction of cosmic rays blcoked by surrounding topography.
hor = 1 - hor;

function [thick, slope] = expSurf(z, rho)
```

SURFACE: Calculates attenuation due to sample thickness

```
%SURFACE
%     SURFACE calculates the correction factor accounting for the
%     thickness of the sample.
%
%     Brent M Goehring
%     2005

att = 155; %g/cm2

%Calculation to determine production rate based on the sample thickness
%based on a simple exponential and an assumed attenuation length of 160
%g/cm2.
if z == 0
   thick = 1;
else
thick = (att / (rho * z)) * (1 - exp(-rho * z / att));
end
```